FISEVIER

Contents lists available at ScienceDirect

Biochimica et Biophysica Acta

journal homepage: www.elsevier.com/locate/bbadis



LRRK2 guides the actin cytoskeleton at growth cones together with ARHGEF7 and Tropomyosin 4



Karina Häbig ^{a,b}, Sandra Gellhaar ^c, Birgit Heim ^a, Verena Djuric ^a, Florian Giesert ^d, Wolfgang Wurst ^{d,e,f,g}, Carolin Walter ^a, Thomas Hentrich ^a, Olaf Riess ^a, Michael Bonin ^{a,b,*}

- ^a Institute of Human Genetics, Department of Medical Genetics, University of Tuebingen, Tuebingen, Germany
- ^b Institute of Human Genetics, MFT Services, University of Tuebingen, Tuebingen, Germany
- ^c Department of Neuroscience, Karolinska Institute, Stockholm, Sweden
- d Institute of Developmental Genetics, Helmholtz Zentrum München, German Research Center for Environmental Health, Neuherberg, Germany
- e Technische Universität München, Lehrstuhl für Entwicklungsgenetik, c/o Helmholtz Zentrum München, Ingolstädter Landstr. 1, 85764 Neuherberg, Germany
- f MPI für Psychiatrie, Kräpelinstr. 2–10, 80804 München, Germany
- g DZNE, German Center for Neurodegenerative Diseases, Munich, Germany

ARTICLE INFO

Article history: Received 23 January 2013 Received in revised form 6 August 2013 Accepted 16 September 2013 Available online 24 September 2013

Keywords: Actin cytoskeleton Parkinson's disease Growth cone Neurite outgrowth

ABSTRACT

Mutations in the *leucine-rich repeat kinase 2 (LRRK2)* gene represent the most common genetic cause of Parkinson's disease (PD). However, LRRK2 function and molecular mechanisms causing the parkinsonian phenotype remain widely unknown. Most of LRRK2 knockdown and overexpression models strengthen the relevance of LRRK2 in regulating neurite outgrowth. We have recently identified ARHGEF7 as the first guanine nucleotide exchange factor (GEF) of LRRK2. This GEF is influencing neurite outgrowth through regulation of actin polymerization. Here, we examined the expression profile of neuroblastoma cells with reduced LRRK2 and ARHGEF7 levels to identify additional partners of LRRK2 in this process. Tropomyosins (TPMs), and in particular TPM4, were the most interesting candidates next to other actin cytoskeleton regulating transcripts in this dataset. Subsequently, enhanced neurite branching was shown using primary hippocampal neurons of LRRK2 knockdown animals. Furthermore, we observed an enhanced number of growth cones per neuron and a mislocalization and dysregulation of ARHGEF7 and TPM4 in these neuronal compartments. Our results reveal a fascinating connection between the neurite outgrowth phenotype of LRRK2 models and the regulation of actin polymerization directing further investigations of LRRK2-related pathogenesis.

© 2013 Published by Elsevier B.V.

1. Introduction

Understanding the molecular mechanisms underlying the pathogenesis of Parkinson's disease (PD) is of major interest in current neuro-degenerative disease research. Especially in Leucine-rich repeat kinase 2 (LRRK2) associated PD, this goal is far from being reached. Up until now, more than 50 variants in this 286 kDa protein have been described [1]. Multiplying the complexity of the research projects, the proven

Abbreviations: F-actin, filamentous actin; G-actin, globular actin; LIMK, LIM domain kinase; LRRK2, leucine-rich repeat kinase 2; PAK, p21 protein (Cdc42/Rac)-activated kinase; qRT-PCR, quantitative reverse transcription polymerase chain reaction; GEF, guanine nucleotide exchange factor; shRNA, short hairpin RNA; siRNA, small interfering RNA; TPM, tropomyosin

* Corresponding author at: Department of Medical Genetics, University Tübingen, Calwerstrasse 7, 72076 Tübingen, Germany. Tel.: +49 7071 29 72295; fax: +49 7071 29 5172

E-mail addresses: Karina.Haebig@med.uni-tuebingen.de (K. Häbig), S.Gellhaar@gmx.de (S. Gellhaar), birgit.heim@medizin.uni-tuebingen.de (B. Heim), verena-djuric@web.de (V. Djuric), florian.giesert@helmholtz-muenchen.de (F. Giesert), wurst@helmholtz-muenchen.de (W. Wurst), carolin.futter@googlemail.com (C. Walter), thomas.hentrich@med.uni-tuebingen.de (T. Hentrich), olaf.riess@med.uni-tuebingen.de (O. Riess), michael.bonin@med.uni-tuebingen.de (M. Bonin).

pathogenic mutations cover all enzymatic domains of this protein. Among those are N1437S/H and R1441C/R/H mutations in the GTPase domain (Roc) of LRRK2 [2–5]. The COR-domain harbours the Y1699C mutation and in the kinase domain the I2020T and the most common G2019S mutation have been found [2,3,6–8]. Additionally, it is not yet clear whether the pathogenicity is being induced by a differentially active GTPase activity or kinase activity of LRRK2, or both.

Research in LRRK2 invertebrate models, cell culture and mouse models clearly indicates an influence of LRRK2 on neurite outgrowth. In *Caenorhabditis elegans* the LRRK2 homologue lrk-1 plays a role in the specification of axons and dendrites, their outgrowth ability and capacity in pathfinding [9,10]. This LRRK2 associated phenotype is supported by analyzing primary murine neurons, in which an enhanced kinase activity of LRRK2 results in reduced neurite growth whereas reduced kinase activity has the opposite consequence of increased neurite outgrowth [11–14].

The molecular basis for this phenotype is far from being fully determined. Investigations on LRRK2 interacting proteins hint at underlying signalling cascades. It has been shown that LRRK2 directly interacts and phosphorylates tubulin leading to more stable yet less dynamic microtubules [15–17]. The interaction of LRRK2 with the elongation factor

 1α (EF1A), known for maintenance of microtubule stability, further supports a function of LRRK2 in this pathway [18]. Axonal guidance, neuronal maintenance and microtubule stabilization are also influenced by the dishevelled protein family (DVL) and the Wnt signalling pathway. Not only the interaction of LRRK2 with DVL1/2/3 was recently identified, but also the expression profile of SH-SY5Y cells with reduced LRRK2 levels and the expression profile of mononuclear cells of PD patients with the G2019S mutation points to a dysregulation of the Wnt signalling pathway [19–21].

In addition to microtubule cytoskeleton structures that are influenced by LRRK2, the impact of LRRK2 on actin cytoskeleton regulation is being heavily investigated. Recently, the interaction of LRRK2 with the Rho GTPases Rac1 and CDC42, that have critical roles in actin cytoskeleton remodelling, was shown by us and others [5,22]. In these studies, the authors identified that LRRK2 attenuates Rac1 activation which in turn causes neurite retraction through disassembly of actin filaments [22]. The influence of LRRK2 on the ratio of filamentous actin (F-actin) to monomeric actin (G-actin) was also shown by the group of M. Ueffing [23]. They identified that LRRK2 is interacting with actin isoforms as well as with proteins that regulate actin stability and maintenance like capping proteins, subunits of the Arp2/3 complex, tropomyosins and actin motor proteins [23]. Additionally, LRRK2 is interacting and phosphorylating ezrin, radixin and moesin that are crucial for the fixation of actin filaments on the cell membrane [16,24].

Together, these hints as well as the expression profile of SH-SY5Y cells after knockdown of LRRK2, clearly point to LRRK2 as a central mediator of the cellular actin network [19]. The detailed analysis of this expression profile highlights a dysregulation of actin cytoskeleton pathways, with ARHGEF7 being one of the most profoundly up-regulated cytoskeletonassociated transcripts. In subsequent studies, ARHGEF7 was identified as the first guanine nucleotide exchange factor (GEF) for the GTPase activity of LRRK2 [5]. This GEF is known to regulate the maintenance of the actin cytoskeleton through (i) regulating the activity of CDC42 and, additionally, (ii) by interacting with PAKs that are important in activating LIMkinases [25,26]. In this study, we further analyzed the interplay of LRRK2 and ARHGEF7 with respect to downstream partners for the actin cytoskeleton signalling. Given that the upregulation of ARHGEF7 leads to enhanced neurite growth [27,28] and the downregulation of LRRK2 results in upregulation of ARHGEF7 [19], the enhanced neurite growth in LRRK2 knockdown models [12,14,29] could be in connection to ARHGEF7 and additional until now not elucidated actin cytoskeleton associated partners.

For that purpose we used the joint downregulation of ARHGEF7 and LRRK2 in SH-SY5Y cells, followed by transcription profiling. By comparing the expression values of the single LRRK2 and the joint knockdown (lower may resemble a rescue effect) we identified four actin associated transcripts that could be relevant for the phenotype. Finally, the results were transferred into *ex vivo* studies to validate their relevance in regulating neurite outgrowth and growth cone morphology.

2. Material and methods

2.1. Antibodies and other reagents

The following antibodies were used in this study: rabbit monoclonal anti-LRRK2 antibody MJFF2 (c41-2) and MJFF3 (c69-6) (Epitomics), rabbit polyclonal anti-SH3 ß-Pix antibody 07-1450 (Millipore), rabbit polyclonal TPM4 antibody ab77683 (Abcam) for detection of mouse TPM4, and mouse monoclonal TPM4 antibody 4E4-102 (Abnova) for detection of human TPM4. Additionally, we used the mouse monoclonal Beta-Actin antibody clone Ac15 (Sigma), the p97 ATPase (VCP) antibody #65278 (Progen) and two different Map2 antibodies (sc20172 Santa Cruz, M1406 Sigma). For the immunofluorescence staining we applied 4',6-diamidino-2-phenylindol (Sigma) to detect nuclei and Alexa Fluor 488 phalloidin (Invitrogen) to visualize the actin cytoskeleton. The coating was done with poly-DL-ornithine hydrobromide (P8638, Sigma) for neurons and with poly-L-lysine (P8920, Sigma) for SH-SY5Y or NIH3T3 cells.

2.2. Cell cultures and mouse model

SH-SY5Y cells (ACC 209) and NIH3T3 (ACC 59) were purchased from DSMZ. The shRNA based LRRK2 knockdown mouse model was published previously [30,31] and kindly provided by the group of W. Wurst (Munich, Germany).

2.3. RNA interference

RNA interference experiments were performed in SH-SY5Y cells according to the previously published protocol [19]. In addition to the published siRNA against LRRK2 (siLRRK2-1) and the control siRNA, we used the siRNA against ARHGEF7 with the target sequence CAAGCGCA AACCTGAACGGAA. Forty eight hours after transfection, the cells were analyzed further.

2.4. RNA isolation, cDNA synthesis and qRT-PCR

RNA was isolated using an RNeasy Mini Kit (Qiagen) according to the protocol. A QuantiTect Reverse Transcription Kit (Qiagen) was used for cDNA synthesis. The primer design for exon–exon boundary-spanning oligonucleotides was done with Primer3 software (http://frodo.wi.mit.edu/primer3/). The used oligonucleotides for the measurement of the human genes are listed in Table 1.

The qRT-PCR was done using a QuantiTect SYBR Green PCR Kit (Qiagen) on the LightCycler 480 (Roche) in a 348-well plate and 10 μ l volume. The PCR settings were applied according to the manufacturer's protocol. The assay specificity was analyzed by melting curves, and standard curves were measured to obtain primer-specific PCR efficiency.

Table 1Oligonucleotides for qRT-PCR measurement, reference genes are displayed in grey.

Gene symbol	Gene name	Forward primer (5'-3')	Reverse primer (5'-3')
PDHB	Pyruvate dehydrogenase beta	ggtttcccattcaagacctg	tggtttccatgtccattggt
GAPDH	Glyceraldehyde-3-phosphate dehydrogenase	agccacatcgctcagacac	gcccaatacgaccaaatcc
SDHA	Succinate dehydrogenase complex, subunit A	agaagccctttgaggagca	cgattacgggtctatattccaga
LRRK2	Leucine-rich repeat kinase 2	atgatgacagcacagctagga	aaacggtcaagcaagattgta
ARHGEF7	Rho guanine nucleotide exchange factor (GEF) 7	ccagcaaatgctcgtacagt	tcactgcagaagggtgattg
ARHGEF9	Cdc42 guanine nucleotide exchange factor (GEF) 9	actcagcagatcaacgaacg	ccgagctcctgtctaggatg
CDC42	Cell division cycle 42	ccagagactgctgaaaagctg	gcacttccttttgggttgag
MGMT	O-6-methylguanine-DNA methyltransferase	ctcttcaccatcccgttttc	agggctgctaattgctggta
NDN	Necdin homolog	tcactgaggagttcgtccaa	ccatgatttgcatcttggtg
SCG5	Secretogranin V (7B2 protein)	tgaagggaggagagacga	gacagacttctttgcaacaaca
SEMA4F	Semaphorin 4F	cagtctgtgcctggagctt	tccaggctctttaggacacaa
SYT1	Synaptotagmin I	tgcaaagtgctgagaaggaa	tgcctccagaatgacaacag
TPM4	tropomyosin 4	tgaaaaggaggacaaatatgaaga	ctttggcctgggcaagtt
ZMAT3	zinc finger, matrin-type	aatcctcagagctgggtcaa	gagagcggggattgaagtaa

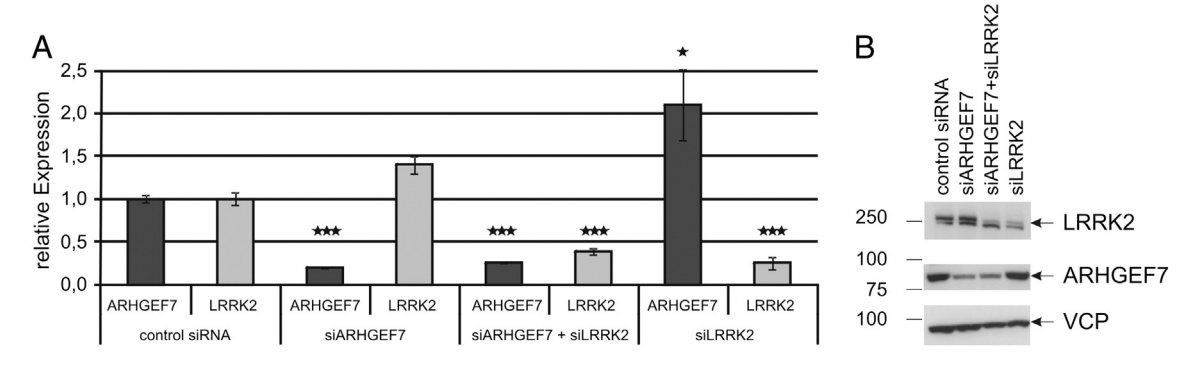


Fig. 1. Efficient knockdown of ARHGEF7 and/or LRRK2 by RNAi. SH-SY5Y cells were transfected with siRNA against LRRK2 and/or ARHGEF7 or control siRNA. A) qRT-PCR measurements were performed to analyze the RNAi efficiency. Relative expression of ARHGEF7 (black) and LRRK2 (grey) was compared to control siRNA transfected cells. PDHB was used as a reference gene for normalization. The analysis was done in 3 independent replicates. Statistics were calculated with Student's t-test, p-value * \leq 0.05, *** \leq 0.001. B) RNAi efficiency test by SDS-Page (6%) followed by immunoblotting of 60 μ g total protein lysate of RNAi transfected cells. Data is representative of three independent experiments. VCP was used as loading control.

For data analysis, the cp-values were generated using a second derivative maximum method. Further data analysis to obtain relative expression values was done with qBASE and PDHB. GAPDH and SDHA were used as reference genes.

2.5. Microarray and pathway analyses

Microarrays were analyzed with biological triplicates for each condition (control siRNA, siARHGEF7, siLRRK2 + siARHGEF7) using the Affymetrix *GeneTitan*® platform with GeneChip® HT HG-U133 + PM array plates. Primary data were analyzed with GeneChip operating software, resulting in quality scores for each array. For normalization, the GCRMA algorithm was applied to all data sets using ArrayAssist Expression Software Version 5.5.1 (Stratagene). To identify differentially regulated genes between the conditions (baseline = control siRNA treatment) we used a filtering scheme of 1.5-fold change in expression

level and p-value of less than 0.05. The results were compared with the previously published data of siLRRK2-treated SH-SY5Y cells [19]. Ingenuity Pathways Analysis software (ingenuity® systems, www.ingenuity.com) was used to generate gene regulation networks, differentially regulated functions and canonical pathways as previously described [19].

2.6. Preparation of hippocampal neurons

For isolation of primary hippocampal neurons, hippocampi were dissected from brains of p0 mice in HBSS. After 14 min of trypsinization (0.25% Trypsin/EDTA) in 37 °C water bath, the hippocampi were washed three times with a Neurobasal-A medium containing $1\times$ Glutamax. Afterwards, two hippocampi per animal were triturated in a 500 μ l plating medium (Neurobasal-A medium with $1\times$ Glutamax, 0.5 ml B27 supplement and 5 ng/ml bFGF). Subsequently the suspension was transferred to coated 6-well plates (Nunc) with coverslips,

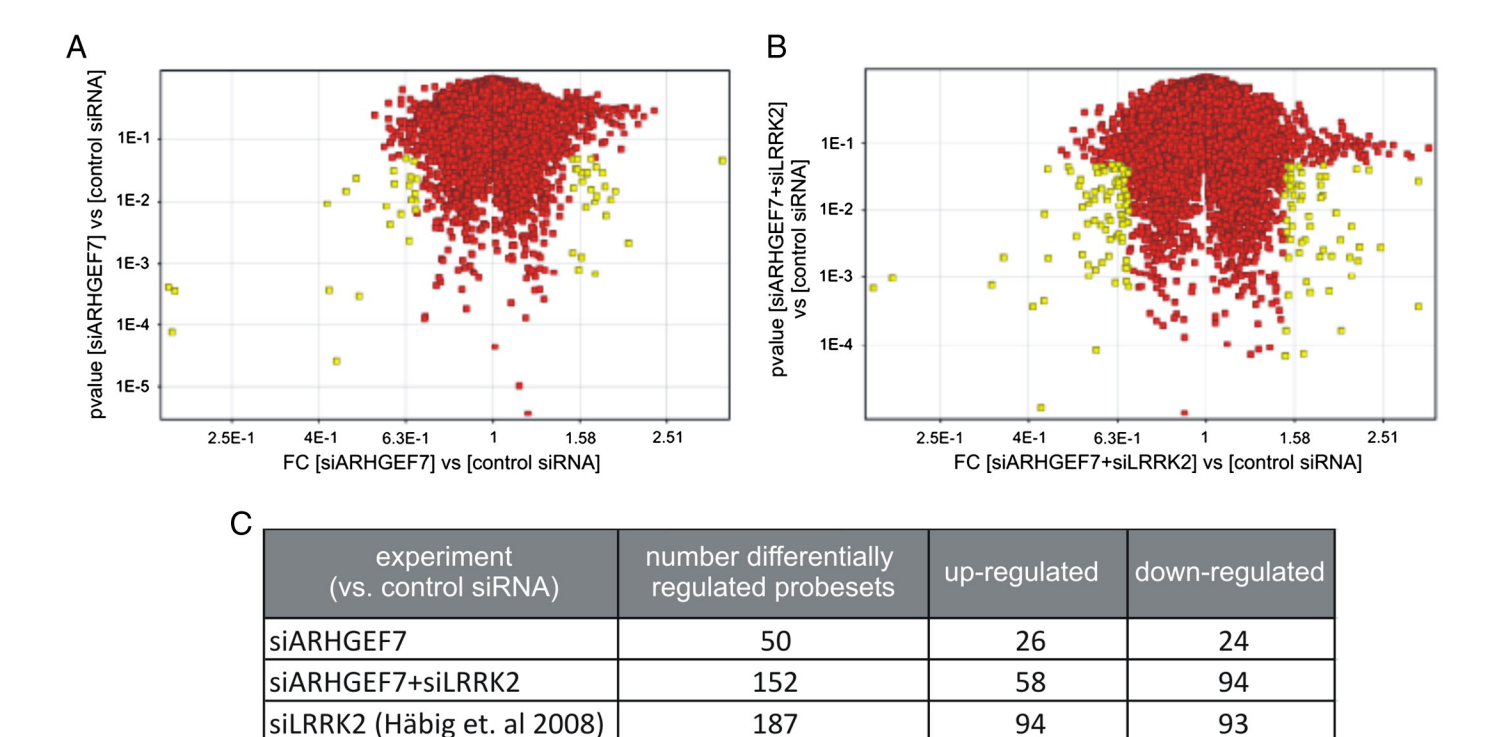


Fig. 2. Differentially regulated transcripts based on the microarray analysis. Volcano plot of the $-\log(p\text{-value})$ against the $\log(\text{fold change})$ of each probeset of A) siARHGEF7 vs. control siRNA, and B) siARHGEF7 + siLRRK2 vs. control siRNA. Grey = all probe sets with p-value ≤ 0.05 and a fold change $\geq \pm 1.5$. C) Overview of the differentially regulated genes (p-value ≤ 0.05 , fold change $\geq \pm 1.5$) of all conditions compared to control siRNA treatment.

containing 2.5 ml of a plating medium. The coating was performed previously for 1 h with 0.5 mg/ml poly-DL-ornithine hydrobromide dissolved in sterile 0.15 M boric acid (with H_2O , pH 8.35, Sigma) and a final three-time-washing step with HBSS. All the reagents were purchased from Gibco unless specified otherwise. After 7 days in culture (DIV7), primary hippocampal neurons were used for analyses.

2.7. Immunofluorescence

The DIV7 hippocampal neurons, SH-SY5Y and NIH3T3 cells, grown on the cover slips, had been prefixated for 2 min with 0.4% PFA in the cell culture media. Subsequently, a fixation step with 4% PFA (in PBS) for 15 min was done followed by incubation overnight at 4 °C in a wet chamber with the primary antibodies (or Alexa Fluor 488 phalloidin for staining the actin cytoskeleton) diluted in PBS with 5% Chemiblocker (Millipore) and 0.1% Triton X-100 (Sigma). After four times of washing with PBS (containing 2% Chemiblocker) the cells were incubated for 2 h at room temperature with a mouse or rabbit secondary Cy2 or Cy3 labelled antibody diluted in PBS (containing 2% Chemiblocker). This was followed by four times of washing with PBS and 10 min of staining of the nuclei with 0.04 µg/ml 4′,6-diamidino-2-phenylindol (in PBS). The digital images from the stained cells were taken with LSM510 (Zeiss) and LSM Image Browser Software (Zeiss).

2.8. Quantification of neurite outgrowth and growth cones

For the quantification of processes, branches and neurite outgrowth, a picture of the indicated number of randomly chosen and separate neurons (Map2 stained) or cells (phalloidin stained) was taken by a person blinded for the condition. For hippocampal neurons at least 3 different litters containing wildtype and knockdown animals were analyzed. The neurite quantification tool of Metamorph 7.6 (Molecular Devices, USA) was applied for the quantification.

The growth cone quantification was done manually for separate phalloidin-stained neurons. First, the mean growth cone number per neuron was quantified. Secondly, the growth cones were grouped accordingly to their shape (collapsed, normal) [32]. Finally, the percentage of neurites of one neuron with collapsed, normal or no growth cone was calculated, followed by the quantification of the average overall neurons of each genotype.

The localization of ARHGEF7 and TPM4 in the growth cones was analyzed with Metamorph 7.6 (Molecular Devices, USA). The indicated numbers of neurons per genotype were examined by a blinded investigator. The area and intensity of ARHGEF7 or TPM4 in the growth cone were determined additional to the area of the entire growth cone (stained with phalloidin). Initially, the area sizes were displayed separately in a scatter plot according to the genotype. For statistical analyses,

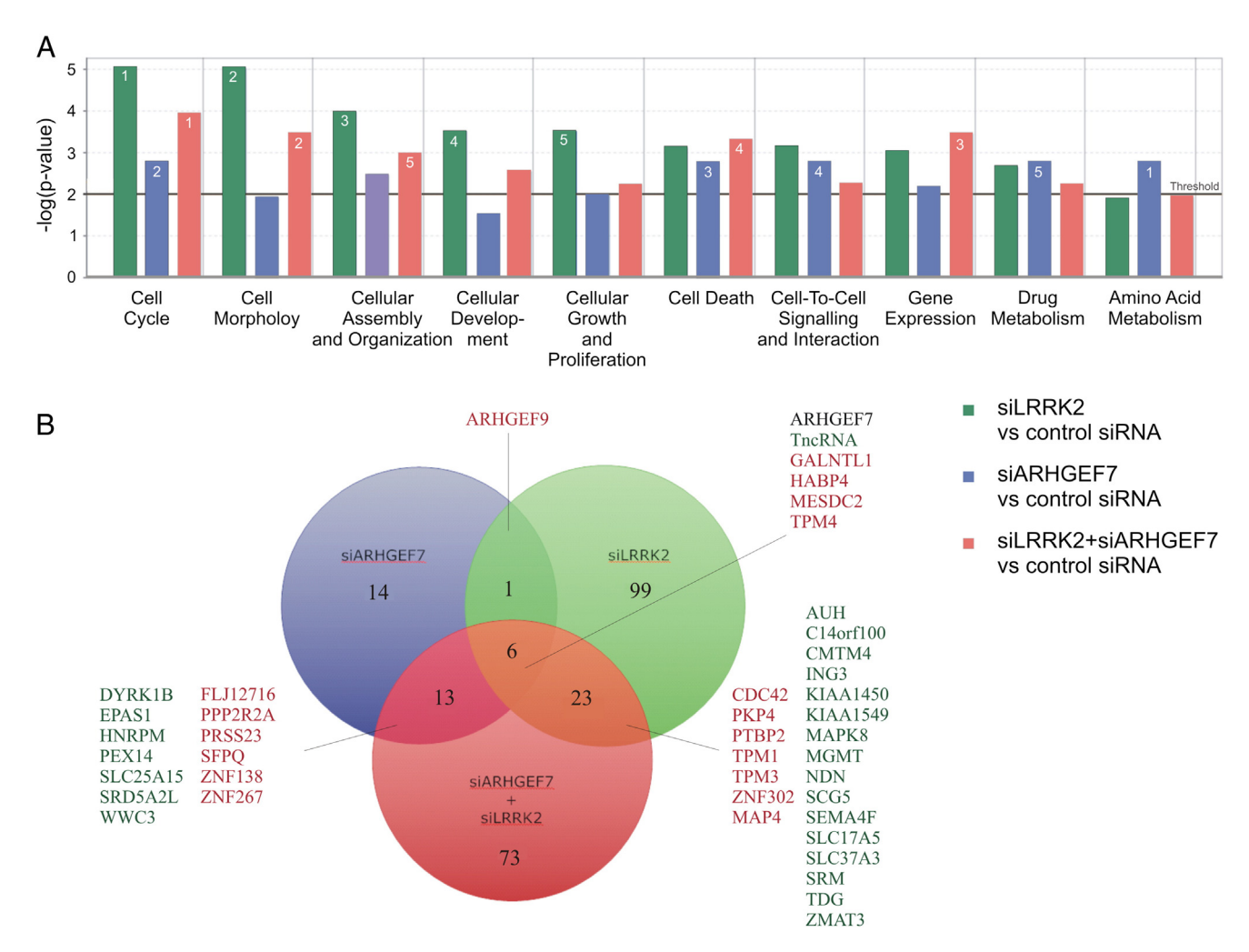


Fig. 3. Comparative analysis of biological functions and transcripts affected by knockdown of ARHGEF7 and/or LRRK2. (A) Ingenuity Pathways Analysis Software was used to compare the datasets of siLRRK2 vs. control siRNA [19], siARHGEF7 vs. control siRNA and siLRRK2 + siARHGEF7 vs. control siRNA. Biological functions are sorted according to the most significant p-value of the siLRK2 dataset. Numbers (1–5) in bars represent the ordered position (most significant = 1) of this function in the dataset. Fischer's exact test was used to calculate the p-values. (B) Venn diagram of siLRRK2 vs. control siRNA [19], siARHGEF7 vs. control siRNA, and siLRRK2 + siARHGEF7 vs. control siRNA. Overlapping transcripts are indicated as up-regulated (red) or down-regulated (green). Black writing represents different direction of regulation in the datasets. 29 overlapping transcripts are regulated by joint RNAi of ARHGEF7 and LRRK2.

the growth cones were grouped according to their size (area of phalloidin), and the ratio of either ARHGEF7 or TPM4 area (or intensity) and the phalloidin area of the growth cones of each group was determined. The averages overall growth cone ratios (grouped) were compared between the genotypes.

The quantification of the F-actin area located around the neuronal cell body was performed with Metamorph 7.6 (Molecular Devices, USA). The cell body area of randomly chosen and separate neurons was calculated using Map2 staining of the neuron. The F-actin area was quantified with the phalloidin staining of the same neuron. The ratio of F-actin area vs. Map2 area was averaged for all the neurons of each genotype.

2.9. Protein isolation and immunoblotting

Protein lysis of whole brain of C57Bl6 wildtype mice for immunoprecipitation studies was performed with 3 ml cell lysis buffer (Cell

Signaling Technologies) containing a protease inhibitor cocktail (Cell Signaling Technologies) and phosphatase inhibitor cocktails II and III (Sigma) using a dounce-homogenisator. After 45 min of incubation with rotation at 4 °C a 15 min centrifugation step at 4 °C at 13,000 rpm was executed. The protein concentration of the supernatant was analyzed with the Bradford method. Protein lysis of the brain regions of C57BI6 wildtype mice was performed as previously described [33]. Thirty micrograms were used for SDS-Page.

Protein lysis for SDS-Page from cultured cells was performed with 100 μ l (per 6-well) of the same lysis buffer and 45 min of incubation with rotation at 4 °C. This was followed by 15 min of centrifugation at 4 °C at 13,000 rpm. Sixty micrograms of total protein lysate were separated on SDS-Page.

After SDS-Page, selected proteins were detected by standard immunoblotting procedures. Quantification of intensities of protein bands was done with the AlphaEaseFCTM software (Alpha Innotech).

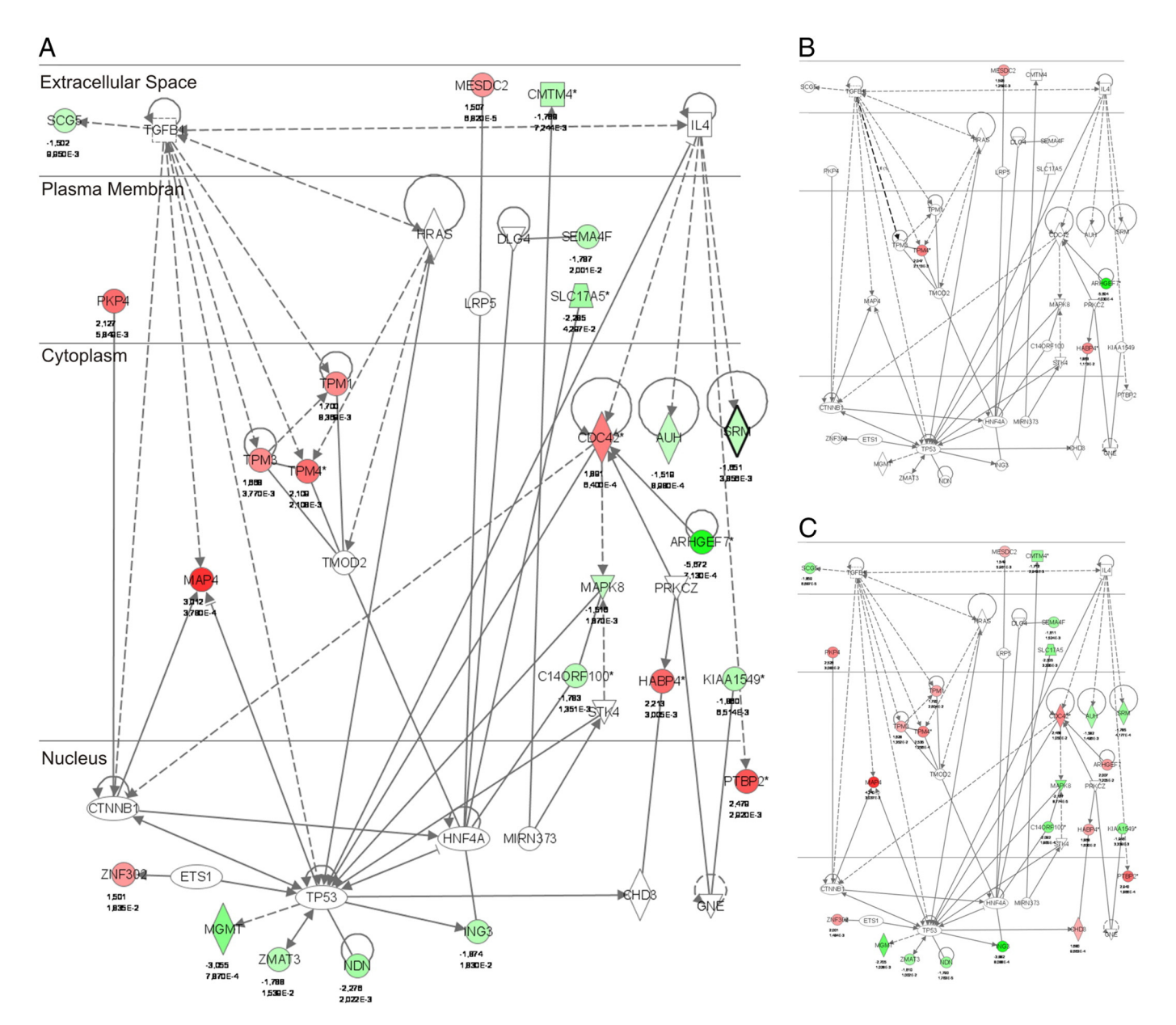
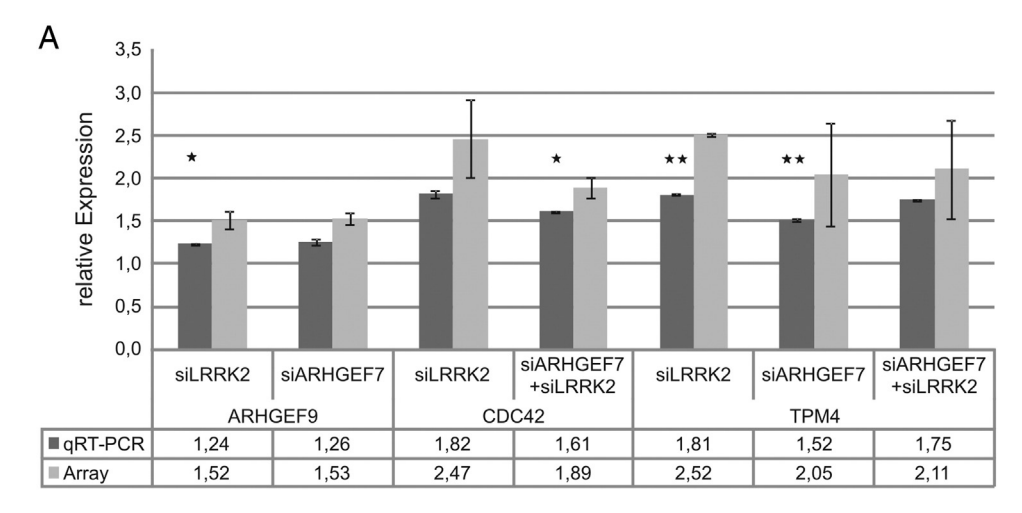
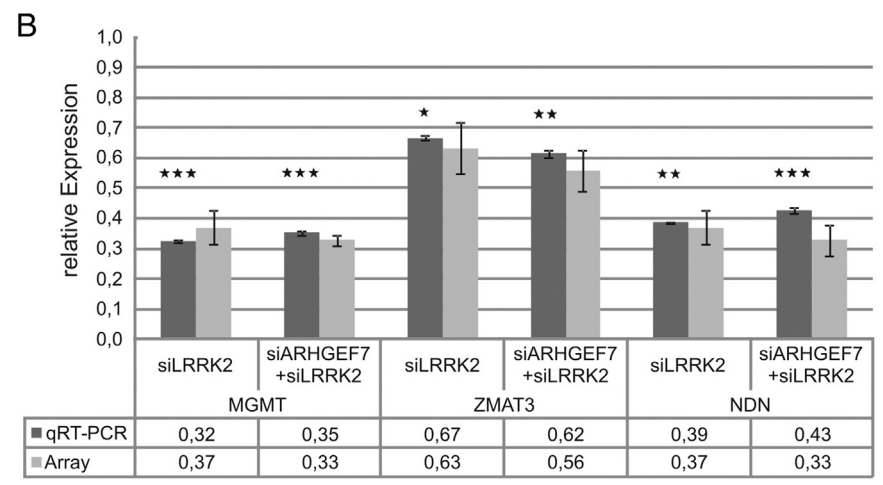


Fig. 4. Pathway of overlapping transcripts from the LRRK2/ARHGEF7 co-knockdown resembles the single LRRK2 knockdown. Gene regulation network established with Ingenuity Pathways Analysis Software contained 39 genes. It is based on 29 differentially regulated transcripts overlapping between the siLRRK2 and the siLRRK2 + siARHGEF7 dataset. The fold change (up-regulated in red, down-regulated in green) and the p-values are shown below the gene symbols. A) LRRK2 + ARHGEF7 co-knockdown. The identical network except the specific expression values is shown for B) ARHGEF7 knockdown and C) LRRK2 knockdown.





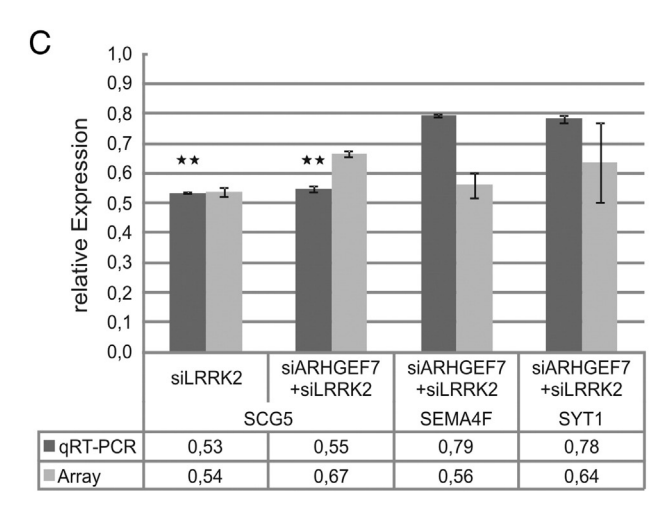


Fig. 5. Validation of microarray data. qRT-PCR measurements for differentially regulated transcripts in at least one of the datasets with known function in A) regulation of the cytoskeleton, B) influence on apoptotic processes, and C) relevance for synaptic regulation or vesicular trafficking. The relative expression values based on microarray (grey) and qRT-PCR (black) data are indicated in the table below. Error bars indicate the standard deviation of the means. The p-value of the microarray data are always \leq 0.05 (not shown) and the p-value of the qRT-PCR data is indicated * \leq 0.05, ** \leq 0.01, *** \leq 0.01 (Student's *t*-test).

3. Results

3.1. Microarray analysis after siRNA mediated co-knockdown of ARHGEF7 and LRRK2

The LRRK2 protein is assumed to play a role in maintaining the actin cytoskeleton. siRNA-mediated knockdown experiments of LRRK2 in a

dopaminergic cell culture model revealed an up-regulation of the guanine nucleotide exchange factor ARHGEF7 [19]. Although the impact of ARHGEF7 on the stability of actin filaments is well known, the interplay of LRRK2 and ARHGEF7 needs to be analyzed in greater detail. Thus, the analysis of signalling cascades after knocking down ARHGEF7 in addition to LRRK2 is one possible step to examine underlying pathways of LRRK2 pathology.

To study the global influence of the double knockdown of both genes we applied microarray analyses. For this purpose we used our previously established LRRK2 knockdown SH-SY5Y cell culture model and transiently transfected siRNA against LRRK2, ARHGEF7 and both together additionally to an unspecific control siRNA. For the knockdown of ARHGEF7 we compared the knockdown capacity of two different siRNAs and chose the more efficient one (data not shown). The knockdown efficiency was controlled on the RNA level by qRT-PCR (Fig. 1A) and on the protein level by Western blot analysis (Fig. 1B). Three independent biological replicates of each condition (control siRNA, siARHGEF7, siLRRK2 + siARHGEF7) were analyzed on Affymetrix GeneChip® HT HG-U133 + PM array plates. All nine arrays passed the quality performance control (Supplementary Fig. 1) and were subsequently used to determine differentially expressed transcripts with a fold change of at least 1.5 and a p-value of <0.05. Comparing ARHGEF7 knockdown and control siRNA treatment yielded in 50 differentially regulated genes (26 up-regulated and 24 down-regulated) (Fig. 2A). Three times more transcripts (152; 58 up-regulated, 94 down-regulated) were differentially expressed in the double knockdown of ARHGEF7 and LRRK2 compared to control siRNA treatment (Fig. 2B). A comparison to the previously published dataset in the same cell line with knockdown of LRRK2 vs. control siRNA transfection is shown in Fig. 2C [19]. Ingenuity pathway analysis was performed with all three available datasets – siLRRK2, siARHGEF7 and siLRRK2 + siARHGEF7 (each of them in comparison to control siRNA treatment). The analysis of the impaired biological pathways (Fig. 3A) points at high similarity between the single knockdown of LRRK2 and the double knockdown of LRRK2 and ARHGEF7, respectively, namely on cell cycle and cell morphology. The knockdown of ARHGEF7 alone resulted in regulation of different biological functions such as amino acid and drug metabolism. Single gene regulation as well as pathway analysis supported the indication that a double knockdown of LRRK2 and ARHGEF7 are very close to the single LRRK2 knockdown (Fig. 3B). The Venn diagram showed an overlap of 7 transcripts that were differentially regulated between siLRRK2 and siARHGEF7 conditions. Considerably more transcripts (19) are overlapping between the single knockdown of ARHGEF7 and the double knockdown of ARHGEF7 and LRRK2. Even more intriguing was the overlap of 29 transcripts between the single knockdown of LRRK2 and the double knockdown of LRRK2 and its GEF. On closer examination of these 29 differentially regulated transcripts, especially considering the altered pathways, one can clearly distinguish between the two single knockdown datasets (Fig. 4B siARHGEF7, Fig. 4C siLRRK2). Contrarily, the double knockdown of LRRK2 and ARHGEF7 (Fig. 4A) was very similar to the single knockdown of LRRK2 (Fig. 4C) looking at the differentially regulated transcripts in the depicted pathways. Although the expression changes were not the same, the direction of regulation was identical.

It is known that both ARHGEF7 and LRRK2 have an impact on the actin cytoskeleton network. ARHGEF7 regulates the actin cytoskeleton through CDC42 and PAKs, whereas LRRK2 influences actin polymerization [23,25,26]. Therefore, it was not surprising that next to apoptosis related transcripts like C14orf100 (also known as Jamp), ING3, MAPK8, MGMT or NDN, the transcript levels of cytoskeleton associated transcripts were most severely changed. Among them were CDC42, MAP4, SEMA4F and several tropomyosins. Comparing the fold change of these cytoskeleton associated transcripts, 66.6% of them are less differentially regulated in the double knockdown of ARHGEF7 and LRRK2 compared to the single knockdown of LRRK2 (Supplementary Fig. 2). The regulation of these transcripts was not initiated by the sole loss of ARHGEF7 as only in the single knockdown of LRRK2 or in the double knockdown of ARHGEF7 and LRRK2 was the change in their expression levels present.

Analysis of selected transcripts by qRT-PCR confirmed the microarray data (Fig. 5). Comparing all the datasets, only six transcripts were regulated in all conditions. One of them is TPM4, a tropomyosin, stabilizing polymeric actin filaments.

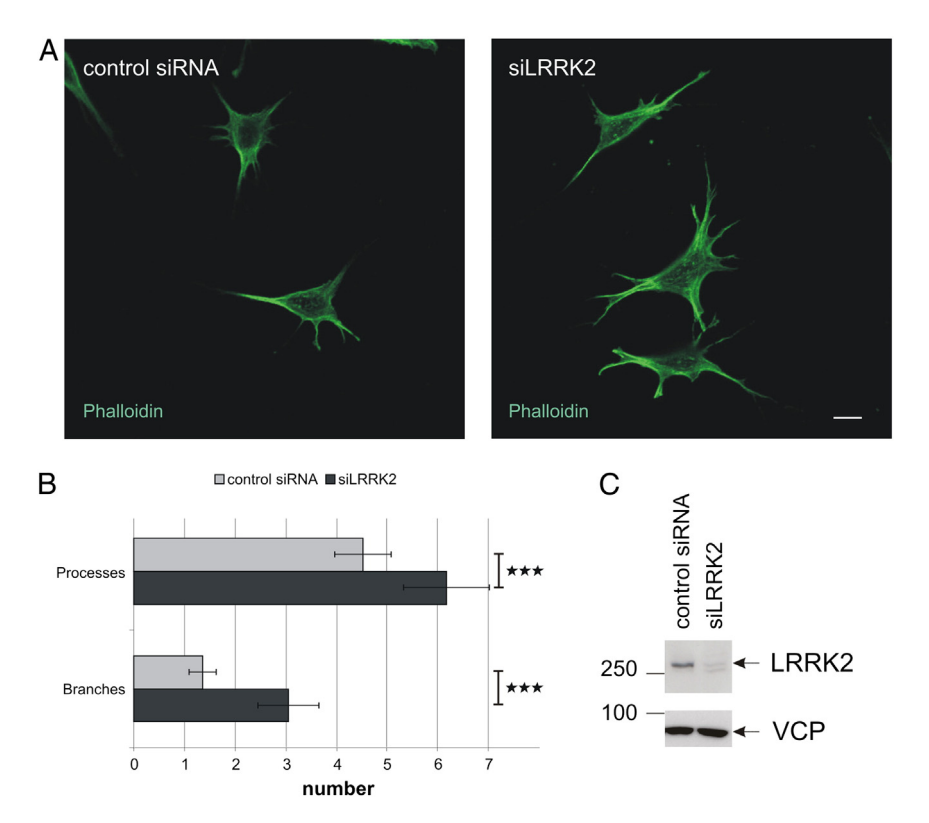


Fig. 6. LRRK2 knockdown leads to an outgrowth phenotype in SH-SY5Y cells. A) Representative image of SH-SY5Y cells treated with control and LRRK2 specific siRNA. F-actin structures stained with phalloidin (green). Scale bar = $10 \mu m$. B) Quantification of processes and branches in control siRNA (n = 77) and siLRRK2 (n = 86) treated SH-SY5Y cells from different transfections. Error bars indicate standard deviation of the means, ***p-value ≤ 0.001 (Student's *t*-test). C) Representative image of LRRK2 knockdown efficiency on the protein level. VCP was used as loading control.

3.2. SH-SY5Y process phenotype was mediated by ARHGEF7 and LRRK2

Neurite growth depends on the fine-tuning of expression and post-transcriptional modification of actin-associated proteins like the small GTPase CDC42, profilins, PAKs and tropomyosins [34]. The underlying mechanisms how LRRK2 is guided to the actin cytoskeleton and how LRRK2 is influencing the actin polymerization, however, are unclear. Similar to other cell culture models [12,35] knocking down LRRK2 in SH-SY5Y cells also features the known outgrowth phenotype with more processes and branches per cell (Fig. 6). This phenotype was

also seen in mouse fibroblasts (NIH3T3) after knockdown of LRRK2 and counting of filopodia (Supplementary Fig. 3). Since knockdown of LRRK2 leads to increased expression of ARHGEF7 and this on its own could already result in enhanced actin polymerization, which could be the fundamental cause for this phenotype, we analyzed the phenotype of the ARHGEF7 knockdown in this SH-SY5Y cell model. As expected, we found a dramatic reduction in the number of processes and branches additionally to a reduction in total outgrowth and length of processes (Fig. 7). To test whether both proteins act together on actin rich structures like processes, neurites or filopodia, we examined the endogenous

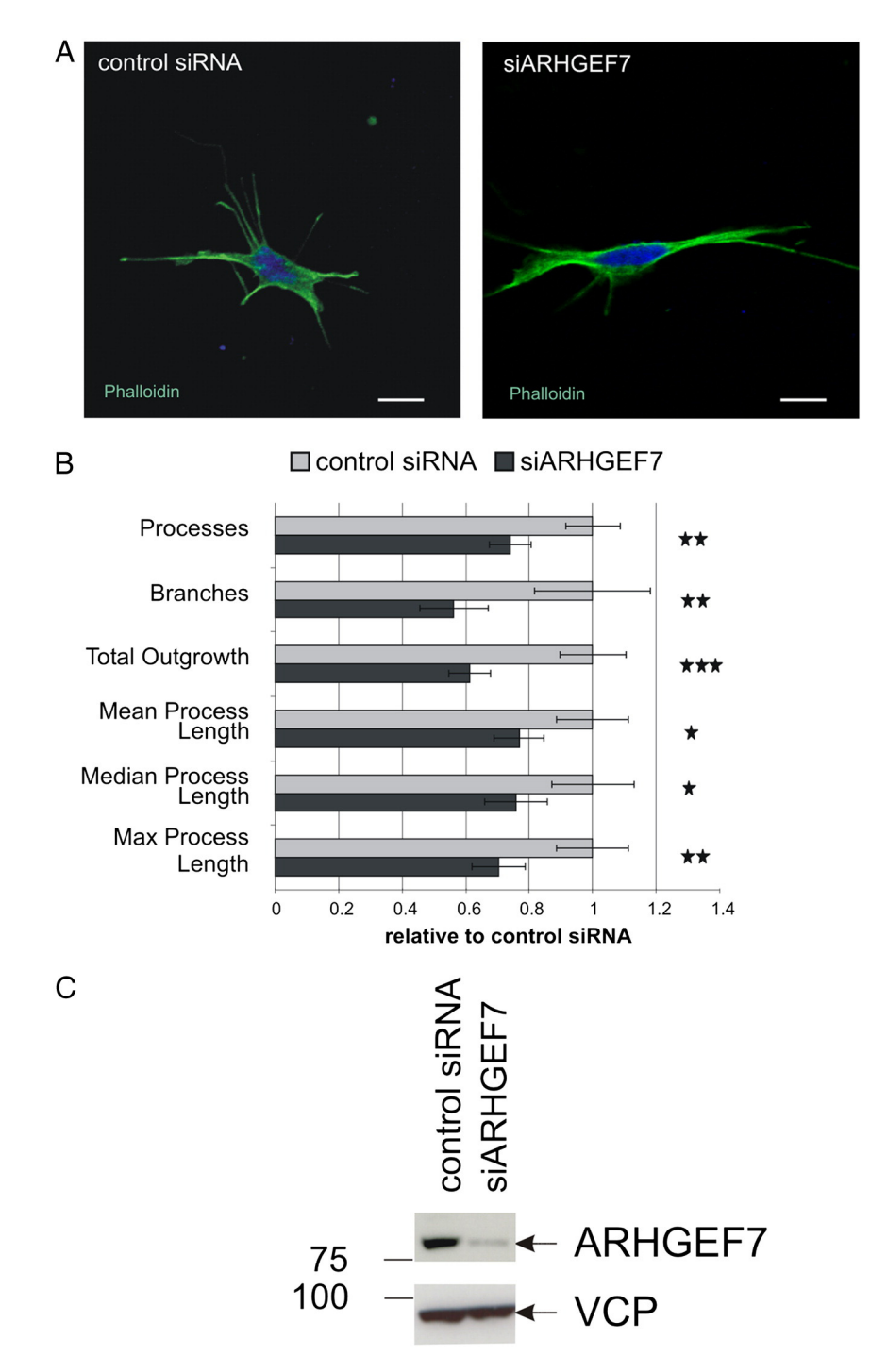


Fig. 7. ARHGEF7 knockdown induces a reverse outgrowth phenotype compared to LRRK2 knockdown. A) Representative image of SH-SY5Y cells treated with control and ARHGEF7-specific siRNA, respectively. F-actin structures stained with phalloidin (green). Scale bar $=10~\mu m$. B) Quantification of process outgrowth in control siRNA-treated (n =53) and siARHGEF7-treated (n =44) SH-SY5Y cells. Error bars indicate standard deviation of the means, *p-value ≤ 0.05 , **p-value ≤ 0.01 , ***p-value ≤ 0.001 (Student's *t*-test). C) Representative image of ARHGEF7 knockdown efficiency on the protein level. VCP was used as loading control.

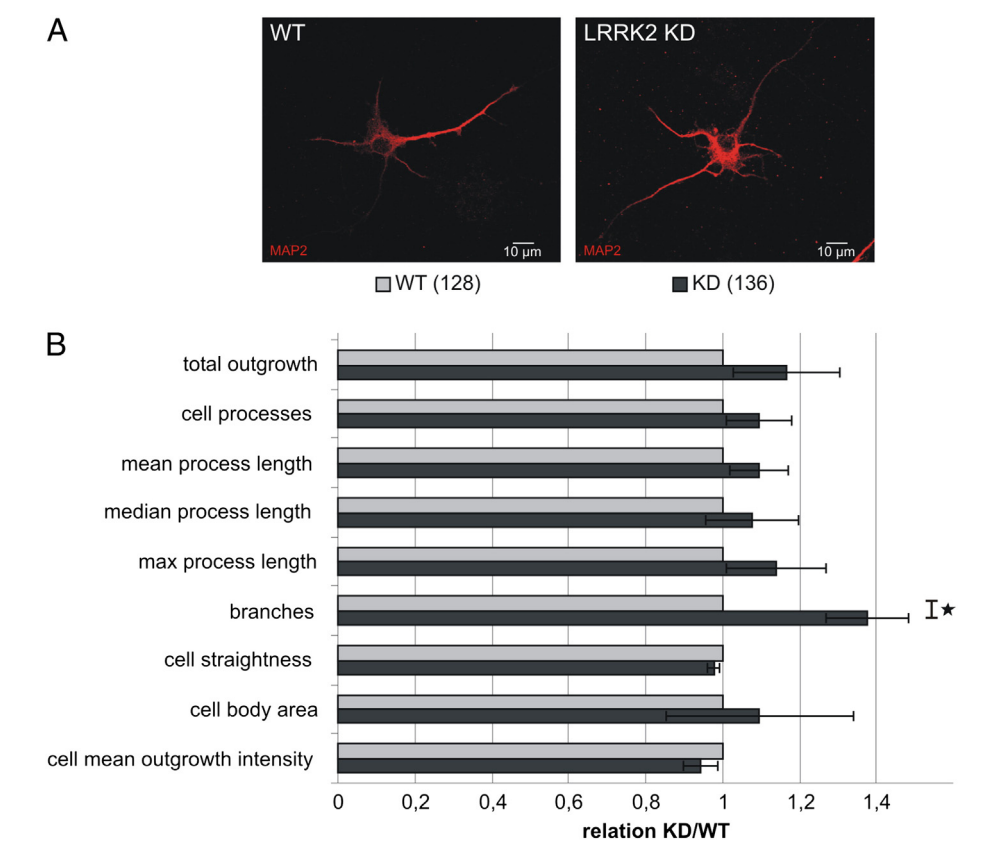


Fig. 8. LRRK2 knockdown leads to enhanced branching of hippocampal neurons. DIV7 hippocampal neurons of LRRK2 knockdown mice (KD) and wildtype (WT) littermates were stained with Map2 (red). A) Representative images of neurons of both genotypes. Scale bar $= 10 \mu m$. B) Wildtype (n = 128) and LRRK2 knockdown (n = 138) neurons of four litters were quantified using the neurite outgrowth tool of Metamorph software. For representative reasons all parameters were normalized to wildtype condition, but the statistical tests were done with the raw data). Error bars indicate standard deviation of the means, *p-value ≤ 0.05 (Student's *t*-test).

localization of both proteins in NIH3T3 cells. These cells express high endogenous levels of LRRK2 which allowed the use of available LRRK2 antibodies generated by the MJFF consortium for immunofluorescence studies. These experiments confirmed the colocalization of LRRK2 and ARHGEF7 in actin rich lamellipodial structures (stained with F-actin, as shown in Supplementary Fig. 4). Also in NIH3T3 cells both proteins were clearly found in the filopodia, in particular at the tips of these actin rich structures (Supplementary Fig. 5).

3.3. LRRK2 knockdown hippocampal neurons were characterized by a growth cone phenotype and enhanced branching

After examining the influence of LRRK2 and ARHGEF7 on processes and branches in cell culture models, we extended our analysis to neuronal cultures. Therefore, we examined primary DIV7 hippocampal neuronal cultures from LRRK2 knockdown mice. The residual amount of LRRK2 expression in whole brain of these LRRK2 knockdown mice is from p0 to p7 less than the barely existent LRRK2 expression in WT mice at p0 (data not shown). Although these mice did not show an obvious dopaminergic neurodegeneration and, thus, no obvious motoric phenotype before adulthood, behaviourally they exhibited subtle motor and sensory phenotypes (personal communication). We found significant enhanced branching of DIV7 LRRK2 knockdown hippocampal neurons (Fig. 8). Co-staining of Map2 and F-actin rich structures and growth cones by phalloidin (Fig. 9A) clearly indicated an enhanced number of growth cones per neuron in the LRRK2 knockdown condition (Fig. 9C). For further characterization of the growth cones, we classified them according to their shape [32]. Neurons of LRRK2 knockdown mice had significantly more normally shaped growth cones at neurite tips. This came along with a reduced number of collapsed growth cones (Fig. 9B). The number of neurites without growth cones was unchanged. The same tendency was observed for growth cones along neurites (Supplementary Fig. 6). Interestingly, hippocampal neurons of LRRK2 knockdown mice showed significantly more F-actin rich structures around the cell soma than the wild types, indicating a potential dysregulation of actin associated proteins (Fig. 9D). Our microarray data clearly pointed on tropomyosins. In particular TPM4, which was not only regulated in all three conditions but also showed a partial rescue effect comparing the single LRRK2 knockdown and the double knockdown of LRRK2 and ARHGEF7 (Supplementary Fig. 2), could be influenced by LRRK2 and ARHGEF7 during F-actin polymerization processes.

TPMs are proteins that stabilize actin filaments and protect them from severing proteins. Although there are more than 40 mammalian tropomyosin isoforms known to date, there is widespread isoform-specific expression in the brain [36]. We analyzed if all the three proteins (LRRK2, ARHGEF7, TPM4) were endogenously expressed in different mouse brain regions (Supplementary Fig. 7). The highest amount of ARHGEF7 and TPM4 was found in the cerebellum while LRRK2 had its highest expression in the striatum. The lowest expression of ARHGEF7 and LRRK2 was found in the brainstem, and TPM4 was lowest in the striatum.

3.4. Phenotype of the LRRK2 knockdown hippocampal neurons was dependent on localization of TPM4 and ARHGEF7

Next, we analyzed whether ARHGEF7 and TPM4 were localized in growth cones and dendrites of hippocampal neurons. As shown in Fig. 10A and B, ARHGEF7 clearly co-localized with Map2 as a marker of dendrites. Additionally, the expression of ARHGEF7 in growth cones, stained with Alexa Fluor 488 phalloidin, was remarkable

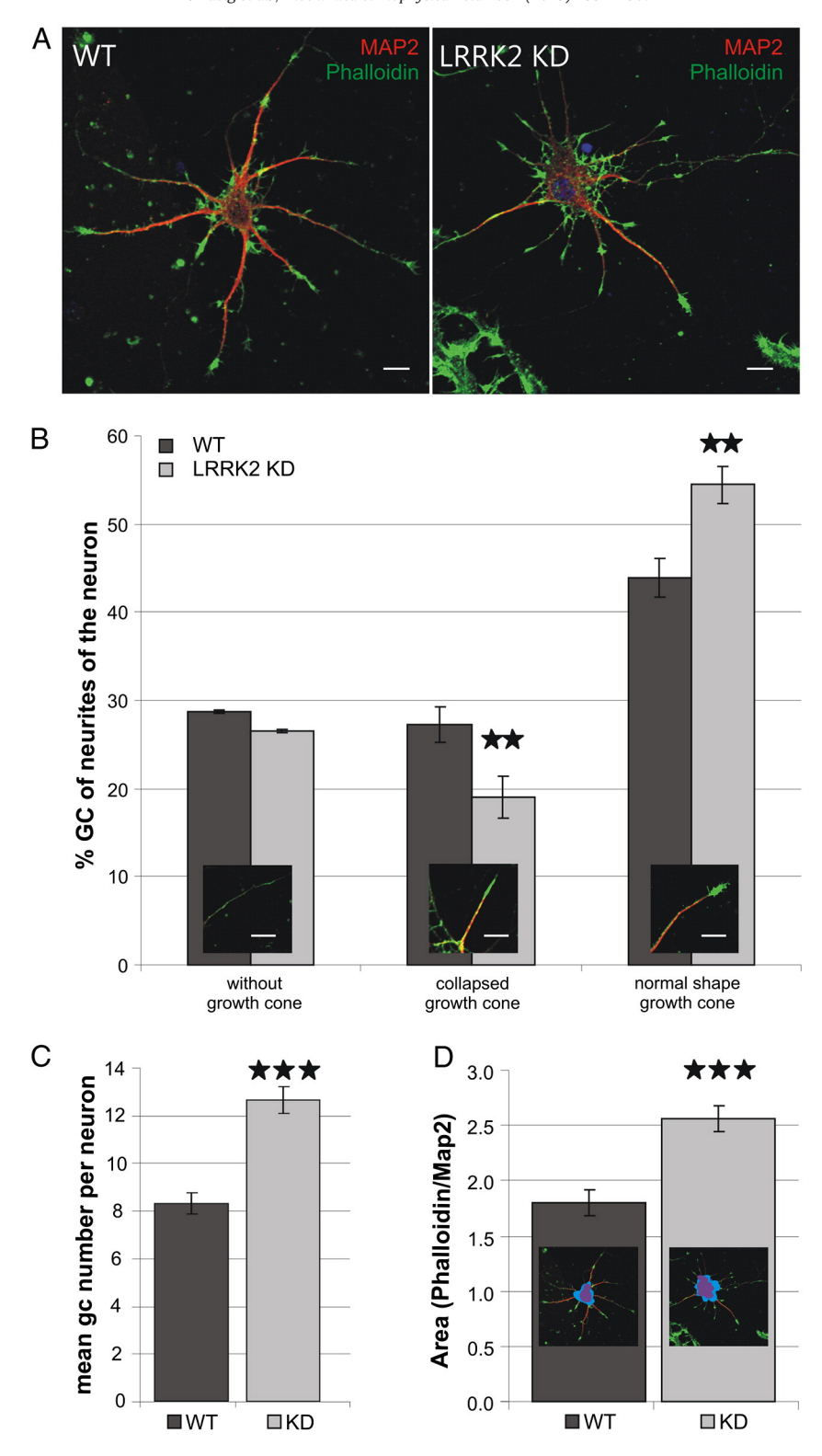


Fig. 9. LRRK2 knockdown induces growth cone phenotype in hippocampal neurons. Growth cones of DIV7 hippocampal neurons of LRRK2 knockdown mice (KD, n=96) and wildtype littermates (WT, n=96) are visualized with phalloidin staining of F-actin (green) structures and co-staining of Map2 (red). A) Representative images of neurons of both genotypes. Scale bar $=10~\mu m$. B) Growth cone morphology of wildtype and LRRK2 knockdown neurons of three litters grouped and quantified according to growth cone shape (representative image as pictured in the bar). C) Mean growth cone number per neuron. D) Area quantification covered by F-actin (phalloidin staining, blue) in relation to the cell body area indicated by Map2 staining (purple) of LRRK2 knockdown neurons (n=30) and wildtype littermates (n=30). Error bars indicate standard deviation of the means, **p-value $\leq 0.01~\mu m$. Student's t-test).

(Fig. 10C, D). Looking at the expression of TPM4 in the same neuronal compartments, the localization of TPM4 in dendrites was predominant to its localization in growth cones (Fig. 11). Because of the low

expression of LRRK2 and the problem of unavailable sensitive antibodies, the endogenous localization of LRRK2 could not be identified in these structures. Yet, the localization of ARHGEF7 and TPM4 in

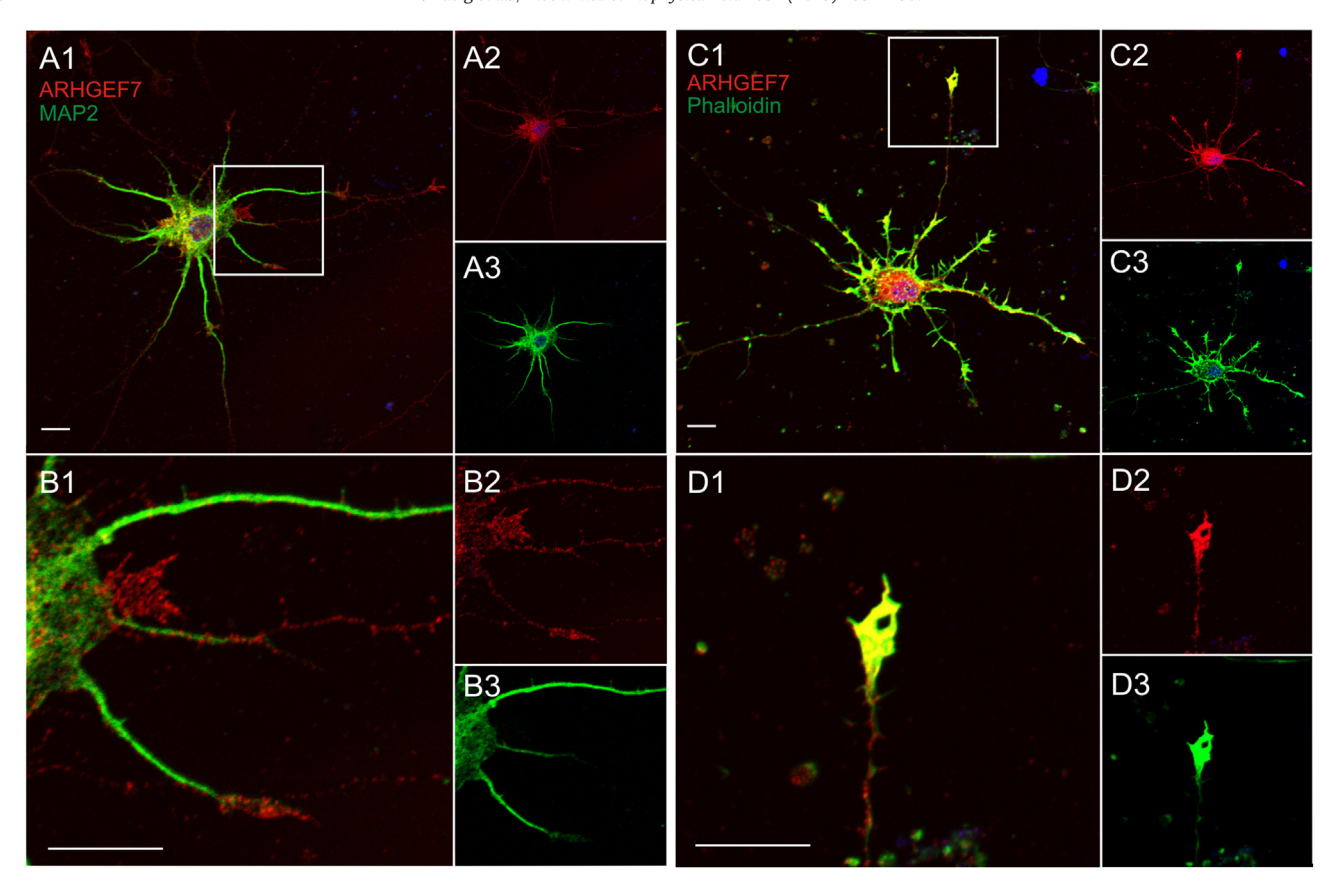


Fig. 10. ARHGEF7 is localized in growth cones and dendrites of hippocampal neurons. Wildtype hippocampal neurons (DIV7) were stained with ARHGEF7 (red) and Map2 (green) (A, B = zoomed box of A) to identify the endogenous localization of ARHGEF7 in dendrites. The co-staining of ARHGEF7 (red) and phalloidin (green) (C, D = zoomed box of C) indicates the co-localization of ARHGEF7 with F-actin rich structures and the growth cone. Scale bar = 10 μm.

dendrites and growth cones led to the hypothesis that both are involved in the LRRK2-associated regulation of the actin-cytoskeleton. Therefore, we compared their localization in hippocampal neurons of LRRK2 knockdown mice with wildtype littermates. The general expression and localization in the neuron were identical for ARHGEF7 (Supplementary Fig. 8) and for TPM4 (Supplementary Fig. 9), respectively.

For a detailed growth cone analysis, we measured their areas (F-actin staining) and blotted them against the areas of the growth cones covered by ARHGEF7 in LRRK2 knockdown compared to wildtype mice (Fig. 12A-C). The results indicated that specifically smaller growth cones (<100 µm²) in LRRK2 knockdown mice had a larger area covered by ARHGEF7 compared to wildtype mice. Group-wise analysis highlighted higher significance of this difference in growth cones <30 μ m² (p-value = 0.0016, Fig. 12D). Despite lower significance, growth cones between 30 μm^2 and 60 μm^2 also showed this enhanced localization of ARHGEF7 (p-value = 0.0066, Fig. 12E). The significant difference then disappeared in growth cones between 60 µm² and 90 μm² (Fig. 12F). The question whether this distribution of ARHGEF7 is accompanied by enhanced ARHGEF7 expression, was answered by calculating the ratio of the ARHGEF7 staining intensity in the growth cone to the corresponding area of phalloidin. Supplementary Fig. 10 points to the same ARHGEF7 intensity in growth cones <30 µm² and less ARHGEF7 intensity in growth cones of 30–60 μm² and 60–90 μm², respectively, comparing LRRK2 knockdown animals with wildtype littermates. These quantifications allow the conclusion that in smaller growth cones, which probably still need to grow and find their direction, loss of LRRK2 leads to enhanced ARHGEF7 expression in an expanded area of growth cones.

The detailed analysis of TPM4 localization in growth cones of hippocampal neurons of LRRK2 knockdown animals indicated an enhanced

TPM4 area per growth cone (Fig. 13A–D). This was accompanied with an increased intensity of TPM4 (Fig. 13E). Looking at the growth cones of LRRK2 knockdown mice with an area of less than 30 μm^2 and of 30 to 60 μm^2 , in which the ARHGEF7 dysregulation was most prominent, the dysregulation of TPM4 was also detected (Supplementary Fig. 11).

4. Discussion

In 2004, the first genetic indication of an involvement of LRRK2 in PD was published [2,3]. Since then the physiological role of LRRK2 has been investigated in different overexpression and knockdown models. There is a growing body of evidence for LRRK2 acting as a direct or indirect regulator of actin polymerization which may provoke the neurite outgrowth phenotype reported in many of the studies [14,23,24]. The underlying molecular mechanisms have, however, remained largely elusive. It has been shown that LRRK2 is interacting with the small GTPases CDC42 and Rac1 [5,22]. Both proteins are key regulators of actin polymerization through activation of the Arp2/3 complex that operates as a seed structure for actin polymerization and for a branched actin network as well [37]. In our previous studies we have shown that an up-regulation of CDC42 after knocking down LRRK2 is associated with an up-regulation of ARHGEF7 in the neuroblastoma cell line SH-SY5Y [19]. ARHGEF7 is a guanine nucleotide exchange factor for both, CDC42 and Rac1, and plays a major role in actin polymerization [25]. Furthermore, ARHGEF7 is influencing PAKs that are important in regulating downstream proteins that maintain F-actin stability, like LIM-kinases and ADF/cofilins [26,38]. As Meixner's group has shown, LRRK2 is influencing the G-actin/F-actin ratio in vitro, but the underlying in vivo mechanisms and the required signalling proteins that lead to the

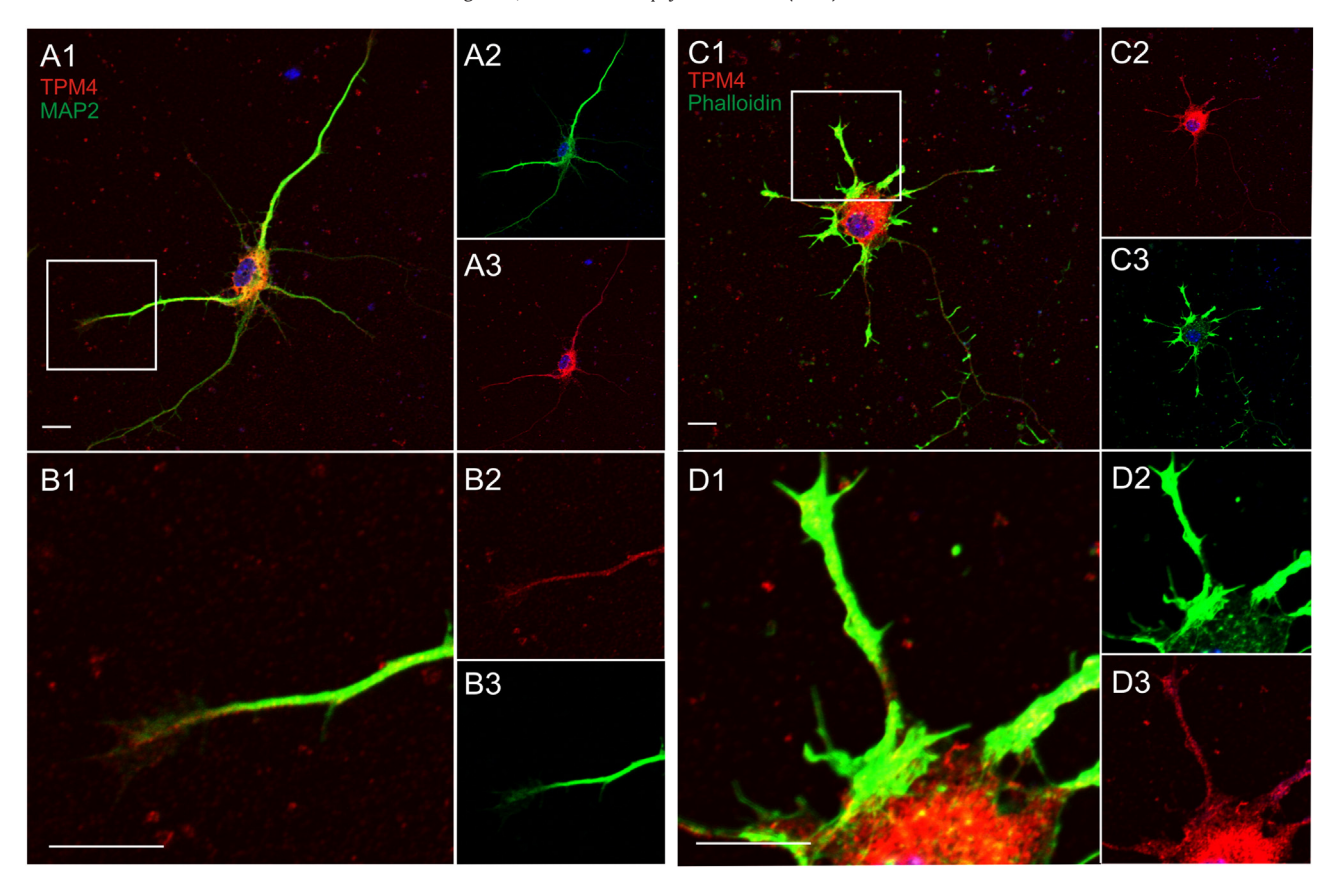


Fig. 11. TPM4 is localized in the growth cones and dendrites of hippocampal neurons. Staining of wildtype hippocampal neurons (DIV7) with TPM4 (red) and Map2 (green) (A, B = zoomed box of A) reveals the localization of TPM4 in dendrites. The staining of TPM4 (red) in addition to phalloidin (green) (C, D = zoomed box of C) points to an expression of TPM4 in growth cones. Scale bar = $10 \mu m$.

described neurite phenotype in LRRK2 models still need to be elucidated [23].

Therefore, the major goal of this study was to characterize the influence of LRRK2 and ARHGEF7 on the regulation of the actin cytoskeleton. We analyzed the transcriptome profile of SH-SY5Y cells with a double knockdown of ARHGEF7 and LRRK2 and compared it to the single knockdown conditions (only ARHGEF7 or LRRK2 knockdown). The knockdown of ARHGEF7 resulted in dysregulation of 50 transcripts. This small number is likely based on a rescue effect of the function of this ARHGEF7 through other GEFs of this family with the same targets. Three times more transcripts were differentially regulated by the double knockdown of LRRK2 and ARHGEF7. These transcripts, their underlying functions and canonical pathways were similar to the observed changes in the transcriptome of the single knockdown of LRRK2 as shown in our previous study [19]. The up-regulation of 3 members of the tropomyosin family in both conditions was particularly interesting. Tropomyosins are coiled-coil dimers that bind actin filaments and stabilize filamentous actin structures against the depolymerization by ADF/ cofilin proteins [36]. More than 40 mammalian tropomyosin isoforms are known that have a broad but isoform-specific expression in the brain [36]. Their expression changes along the differentiation process of neurons [39]. Additionally, TPM5 and TPM1 influence neuronal branching [40-43]. Since the TPM4 isoform is differentially regulated in the transcriptome of all the three knockdown conditions, we prioritized the analyses of LRRK2, ARHGEF7 and TPM4 in different LRRK2 knockdown models.

The LRRK2 knockdown induced phenotype of SH-SY5Y cells manifested in more processes and enhanced branching. This observation reflects the known phenotype of LRRK2 knockout neurons and of

PC12 cells with reduced LRRK2 levels [12,14,29,38], although some studies come to opposing results [15,23].

The overexpression of G2019S LRRK2 in primary neurons as well as in the SH-SY5Y cell line has been described with the opposite phenotype characterized by reduced neurite length [11-14,22]. The same phenotype has been detected in LRRK2 models with mutations in the GTPase domain [12,44,45]. The enhanced process and branching phenotype of the SH-SY5Y LRRK2 knockdown cells coincided with enhanced ARHGEF7 expression. This raised the question whether the increased expression of ARHGEF7 could be responsible for the phenotype. Previous publications showed that both, the overexpression of full length ARHGEF7 results in increased neuritogenesis and the reverse phenotype with degeneration of neurites is induced by overexpression of mutated ARHGEF7 without GEF activity [27,28]. The down-regulation of ARHGEF7 in our experiments led to a strong reduction of all neurite outgrowth parameters, which verified the previous published data. Moreover, the expression changes of several cytoskeleton associated transcripts in the LRRK2 knockdown condition could be partially rescued by the additional knockdown of ARHGEF7.

In NIH3T3 cells, we now clearly showed that both LRRK2 and ARHGEF7 were expressed in F-actin rich lamellipodia and filopodia — the structures in which outgrowth is occurring in fibroblasts. Since ARHGEF7 is known to be a GEF of LRRK2 [5] it needs to be determined if the causing factor for the primary outgrowth phenotype is based on the loss of LRRK2, the overexpression of ARHGEF7 or a combination of both

The analysis of primary neurons of a LRRK2 knockdown mouse was chosen as a model to solve this question. We used our previously published shRNA based LRRK2 mouse model as the source for the neurons

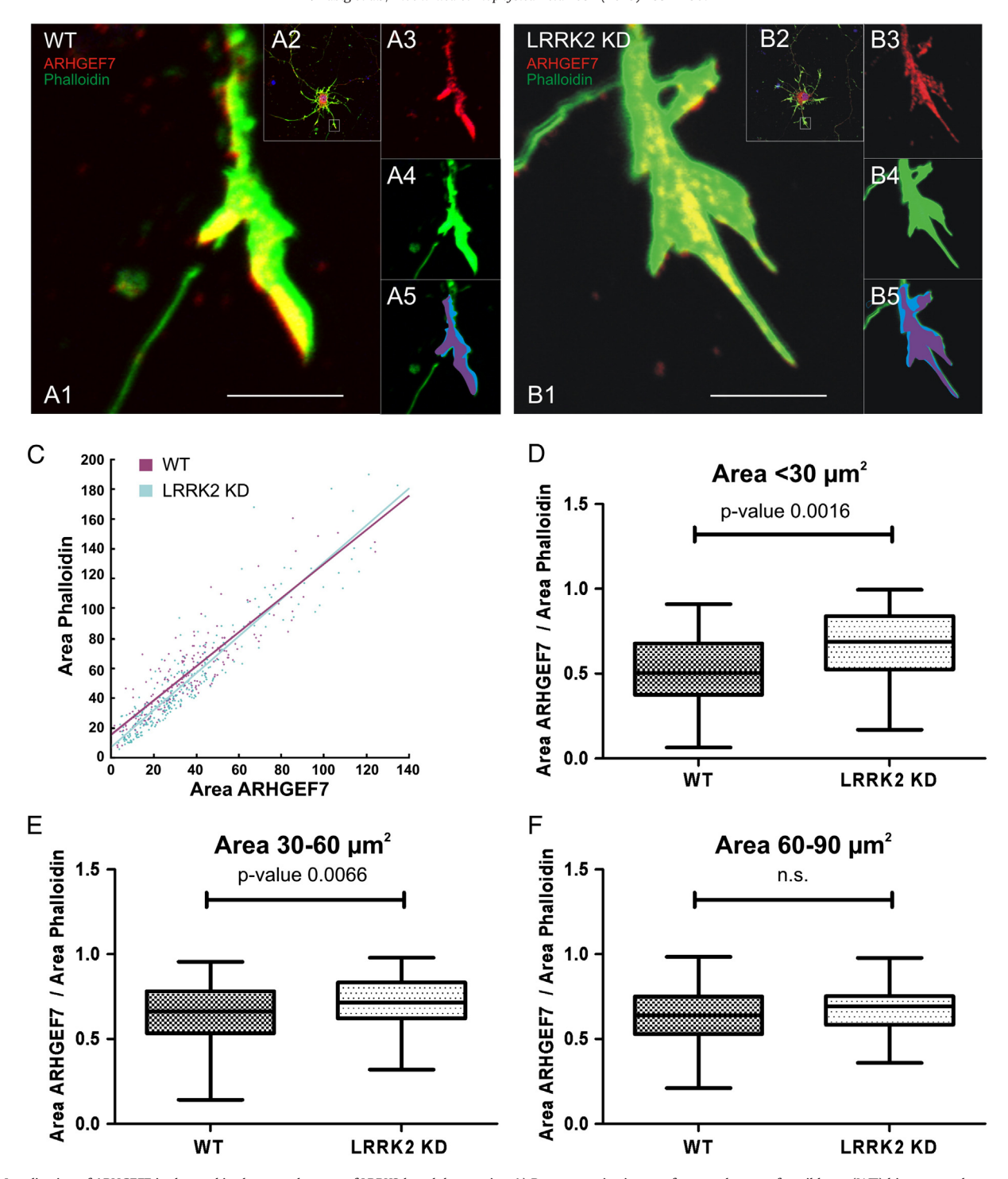


Fig. 12. Localization of ARHGEF7 is changed in the growth cones of LRRK2 knockdown mice. A) Representative image of a growth cone of a wildtype (WT) hippocampal neuron (DIV7) (overview A1, A2) stained with ARHGEF7 (red, A3) and phalloidin (green, A4). Area quantification with Metamorph 7.6 (Molecular Devices, USA) (A5, ARHGEF7 area = purple, phalloidin area = blue). Scale bar = 5 μ m. B) Representative image of a LRRK2 knockdown (KD) growth cone, colouring same as in A. C) Scatter plot of the phalloidin growth cone area and the ARHGEF7 growth cone area of 201 wildtype growth cones (of 28 neurons, purple) and 273 LRRK2 knockdown growth cones (of 30 neurons, blue). D–F) Box plots of the quantification of the growth cone area (ARHGEF7/phalloidin) grouped according to the growth cone area. Indicated are the median, the lower and upper quartiles and the minimum and maximum of the data. (D = phalloidin area of \leq 30 μ m², E = phalloidin area of \leq 30 μ m², E = phalloidin area of \leq 30 μ m², E = phalloidin area of \leq 30 μ m².

[30,31]. In DIV7 primary hippocampal neurons we identified enhanced branching, a phenotype known from other LRRK2 knockout or knockdown models [12,14,29]. Additionally, we identified both, an increased number of growth cones per neuron and a reduced number of collapsed growth cones confirming that neurons derived from these mice recapitulate important features of LRRK2 deficiency. In the neurons of these mice, the F-actin area around the cell body was also expanded, suggesting that

the dysregulation of TPM4 and ARHGEF7 after knocking down LRRK2 is the cause. Supporting this hypothesis, we identified a co-localization of both proteins, additionally to LRRK2, in the main brain areas (cortex, cerebellum, hippocampus, brainstem, and striatum). The subcellular localization of TPM4 and ARHGEF7 in primary hippocampal neurons of wildtype mice is in dendrites and growth cones, with a more pronounced expression of ARHGEF7 in growth cones when compared to TPM4.

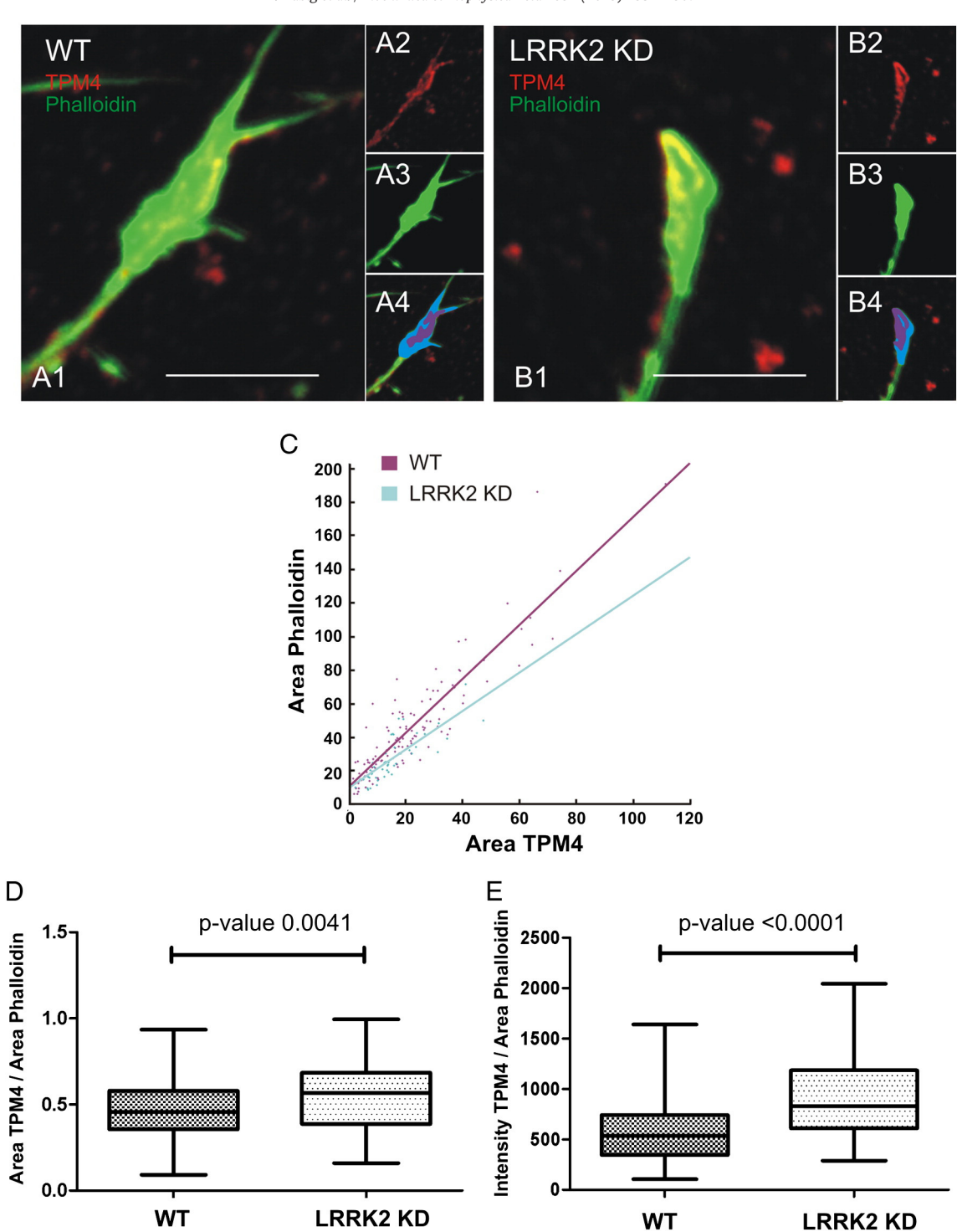


Fig. 13. Localization and intensity of TPM4 is changed in the growth cones of LRRK2 knockdown mice. A) Representative growth cone image of a wildtype (WT) hippocampal neuron (DIV7) (overview A1) stained with TPM4 (red, A2) and phalloidin (green, A3). Area quantification done with Metamorph 7.6 (Molecular Devices, USA) (A4, TPM4 area = purple, phalloidin area = blue). Scale bar = 5 µm. B) Representative image of a LRRK2 knockdown (KD) growth cone, staining same as in A. C) Scatter plot of the phalloidin-stained growth cone area and the TPM4-stained growth cone area of 118 wildtype growth cones (of 48 neurons, purple) and 48 LRRK2 knockdown growth cones (of 7 neurons, blue). D) Box plot of the growth cone area covered by TPM4 (TPM4 area/phalloidin area) of the growth cones shown in C. E) Quantification of TPM4 intensity per growth cone (TPM4 area/phalloidin area) of the growth cones shown in C. Indicated are the median, the lower and upper quartiles and the minimum and maximum of the data. Statistics = Student's 1-test.

In primary neurons of rats, TPM4 is located in the growth cone bodies and tips of filopodia [46]. In this study Had et al. postulated that TPM4 may be involved in the motile events of neurite growth and synaptic plasticity through its involvement in stabilizing the spatial organization of the filamentous actin and its binding partners. Although nothing is known about TPM4 and its direct influence in branching,

the expression of another tropomyosin TPM5 leads to enlarged growth cones and enhanced branching [40].

As tropomyosins, ARHGEF7 has important functions in growth cones as well. Studies in PC12 cells point out that in response to bFGF2 the Ras/ERK cascade gets activated and phosphorylates ARHGEF7. Subsequently, ARHGEF7 is translocated to neuronal growth cones, which is important

for neurite outgrowth [47]. The impact of LRRK2 on the ERK cascade is currently actively investigated in detail by different groups, but until now it is not clear whether or not LRRK2 is able to directly activate the ERK cascade [13,35,48,49]. In fact, the MEK inhibitor UO126 rescued the neurite shortening phenotype of differentiated G2019S SH-SY5Y cells, indicating an influence of the ERK pathway on the phenotype [13]. Previously, we have clearly shown, that LRRK2 is able to directly phosphorylate ARHGEF7 at two positions, but these target sites are not the same as the one phosphorylated by the Ras/ERK cascade [5,47]. Additionally, the knockdown of LRRK2 leads to enhanced expression of FGF2 [19], a protein which is known to induced neurite branching [50,51].

Our hypothesis that TPM4 and ARHGEF7 are responsible for the neurite branching and the growth cone phenotype of LRRK2 knockdown neurons is supported by the detailed comparison of growth cones of LRRK2 knockdown and wildtype neurons, respectively. We identified higher ARHGEF7 levels and enhanced growth cone area covered by ARGHEF7 in small growth cones of LRRK2 knockdown hippocampal neurons. The same elevated intensity and area was identified through TPM4 staining. Given that growth cone motility and morphology are closely related to neurite branching events [50,52], dysregulation of ARHGEF7 and TPM4 in this neuronal compartment, may be responsible branching phenotype of LRRK2 knockdown neurites.

Based on our results and those of previous studies, we favour the following model, which needs extensive experimental validation:

Under normal conditions, LRRK2 may act as a scaffolding protein bound to F-actin structures. It further guides TPM4, crucial for the actin stability, and ARHGEF7, important for activating CDC42 and PAKs to the actin cytoskeleton. Through its own activity and interacting partners, LRRK2 regulates the balance between stabilization and destabilization of F-actin structures.

Probably, loss of LRRK2 as observed in our model leads to upregulation and/or mislocalization of ARHGEF7 and TPM4, especially in growth cones. Altered ARHGEF7 expression may hence cause an enhanced activation of CDC42, which in turn leads to more filamentous actin. Furthermore, ARHGEF7 may activate PAKs resulting in a reduced F-actin destabilizing impact of ADF/Cofilin. More available TPM4 in growth cones may stabilize newly synthesized actin filaments. The joint action of ARHGEF7 and TPM4 probably causes an altered growth rate of actin filaments at the barbed end and fragmentation of actin filaments at the pointed end, leading to enhanced neurite outgrowth with more growth cones and branching under LRRK2 deficiency.

This scenario is supported by the known interaction partners of LRRK2. First, LRRK2 is able to interact with different actin isoforms [18,23]. Second, tropomyosins are extensively investigated as interacting and stabilizing proteins of actin [36], and accessorily TPM isoforms are identified as interacting partners of LRRK2 [23]. And third, ARHGEF7 activates the GTPase activity of LRRK2 through its GEF function and direct interaction with LRRK2 [5].

While awaiting experimental proof, our model could also be expanded to speculate on the molecular mechanism leading to PD pathogenesis. Potentially, mutated and thereby more active LRRK2 binds less TPM4. That could result in less available TPM4 for F-actin binding and stabilization. Additionally, the binding of mutated LRRK2 to ARHGEF7 and/or CDC42 could be reduced, as shown for the R1441C LRRK2 variant and ARHGEF7 [5]. In doing so, the balance between CDC42 activity and F-actin polymerisation could be massively perturbed. This would result in reduced neurite outgrowth with destabilization of actin filaments, probably in aged patients without any molecular rescue effect.

5. Conclusion

Our results support the impact of LRRK2 on the regulation of actin cytoskeleton signalling. By expanding the microarray based *in vitro* analysis to *ex vivo* experiments in neurons; we broaden the insights in the LRRK2 associated regulation of ARHGEF7 and TPM4 in growth cones. The complex interplay of LRRK2, ARHGEF7, and TPM4 needs to

be further elucidated to examine its relevance with respect to PD pathogenesis. The cooperation between the three actin cytoskeleton-associated proteins could be part of a molecular pathway which is responsible for the neurite outgrowth phenotype of LRRK2 models.

Supplementary data to this article can be found online at http://dx. doi.org/10.1016/j.bbadis.2013.09.009.

Conflict of interest

The authors declare no conflict of interest.

Acknowledgements

We would like to thank the members of the Transgenic Facility Tübingen for the animal care. Additionally, we thank J. Prechtel and S. Poths for processing the microarrays (Microarray Facility Tübingen, www.mftservices.de). We thank C.J. Gloeckner and D. Vogt Weisenhorn for their helpful comments. This work was supported by Fortüne grant 2023-0-0 to KH, FP7 program MEFOPA to MB and by the Deutsche Forschungsgemeinschaft (SFB596), the Federal Ministry of Education and Research (National Genome Research Network, 01GS08174), the Helmholtz Association and the Helmholtz Alliance "Mental Health in an Ageing Society" (HELMA).

Ethical standards

The consent was written and approved by the "Ethikkommission der Universität Tübingen". The experiments comply with the current laws in Germany.

References

- C. Paisan-Ruiz, LRRK2 gene variation and its contribution to Parkinson disease, Hum. Mutat. 30 (2009) 1153–1160.
- [2] A. Zimprich, S. Biskup, P. Leitner, P. Lichtner, M. Farrer, S. Lincoln, J. Kachergus, M. Hulihan, R.J. Uitti, D.B. Calne, A.J. Stoessl, R.F. Pfeiffer, N. Patenge, I.C. Carbajal, P. Vieregge, F. Asmus, B. Muller-Myhsok, D.W. Dickson, T. Meitinger, T.M. Strom, Z.K. Wszolek, T. Gasser, Mutations in LRRK2 cause autosomal-dominant parkinsonism with pleomorphic pathology, Neuron 44 (2004) 601–607.
- [3] C. Paisan-Ruiz, S. Jain, E.W. Evans, W.P. Gilks, J. Simon, M. van der Brug, A. Lopez de Munain, S. Aparicio, A.M. Gil, N. Khan, J. Johnson, J.R. Martinez, D. Nicholl, I.M. Carrera, A.S. Pena, R. de Silva, A. Lees, J.F. Marti-Masso, J. Perez-Tur, N.W. Wood, A.B. Singleton, Cloning of the gene containing mutations that cause PARK8-linked Parkinson's disease, Neuron 44 (2004) 595–600.
- [4] J.O. Aasly, C. Vilarino-Guell, J.C. Dachsel, P.J. Webber, A.B. West, K. Haugarvoll, K.K. Johansen, M. Toft, J.G. Nutt, H. Payami, J.M. Kachergus, S.J. Lincoln, A. Felic, C. Wider, A.I. Soto-Ortolaza, S.A. Cobb, L.R. White, O.A. Ross, M.J. Farrer, Novel pathogenic LRRK2 p.Asn1437His substitution in familial Parkinson's disease, Mov. Disord. 25 (13) (2010 Oct 15) 2156–2163, http://dx.doi.org/10.1002/mds.23265.
- [5] K. Haebig, C.J. Gloeckner, M.G. Miralles, F. Gillardon, C. Schulte, O. Riess, M. Ueffing, S. Biskup, M. Bonin, ARHGEF7 (Beta-PIX) acts as guanine nucleotide exchange factor for leucine-rich repeat kinase 2, PLoS One 5 (2010) e13762.
- [6] W.C. Nichols, N. Pankratz, D. Hernandez, C. Paisan-Ruiz, S. Jain, C.A. Halter, V.E. Michaels, T. Reed, A. Rudolph, C.W. Shults, A. Singleton, T. Foroud, Genetic screening for a single common LRRK2 mutation in familial Parkinson's disease, Lancet 365 (2005) 410–412.
- [7] A. Di Fonzo, C.F. Rohe, J. Ferreira, H.F. Chien, L. Vacca, F. Stocchi, L. Guedes, E. Fabrizio, M. Manfredi, N. Vanacore, S. Goldwurm, G. Breedveld, C. Sampaio, G. Meco, E. Barbosa, B.A. Oostra, V. Bonifati, A frequent LRRK2 gene mutation associated with autosomal dominant Parkinson's disease, Lancet 365 (2005) 412–415.
- [8] W.P. Gilks, P.M. Abou-Sleiman, S. Gandhi, S. Jain, A. Singleton, A.J. Lees, K. Shaw, K.P. Bhatia, V. Bonifati, N.P. Quinn, J. Lynch, D.G. Healy, J.L. Holton, T. Revesz, N.W. Wood, A common LRRK2 mutation in idiopathic Parkinson's disease, Lancet 365 (2005) 415–416.
- [9] J. Samann, J. Hegermann, E.V. Gromoff, S. Eimer, R. Baumeister, E. Schmidt, Caenorhabditis elegans LRK-1 and PINK-1 act antagonistically in stress response and neurite outgrowth, J. Biol. Chem. 284 (24) (2009 Jun 12) 16482–16491, http://dx.doi.org/10.1074/jbc.M808255200. Epub 2009 Feb 27.
- [10] A. Sakaguchi-Nakashima, J.Y. Meir, Y. Jin, K. Matsumoto, N. Hisamoto, LRK-1, a C. elegans PARK8-related kinase, regulates axonal-dendritic polarity of SV proteins, Curr. Biol. 17 (2007) 592–598.
- [11] B. Winner, H.L. Melrose, C. Zhao, K.M. Hinkle, M. Yue, C. Kent, A.T. Braithwaite, S. Ogholikhan, R. Aigner, J. Winkler, M.J. Farrer, F.H. Gage, Adult neurogenesis and neurite outgrowth are impaired in LRRK2 G2019S mice, Neurobiol. Dis. 41 (2011) 706–716.
- [12] D. MacLeod, J. Dowman, R. Hammond, T. Leete, K. Inoue, A. Abeliovich, The familial Parkinsonism gene LRRK2 regulates neurite process morphology, Neuron 52 (2006) 587–593.
- [13] E.D. Plowey, S.J. Cherra III, Y.J. Liu, C.T. Chu, Role of autophagy in G2019S-LRRK2-associated neurite shortening in differentiated SH-SY5Y cells, J. Neurochem. 105 (3) (2008 May) 1048–1056, http://dx.doi.org/10.1111/j.1471-4159.2008. 05217.x. Epub 2008 Jan 7.

- [14] J.C. Dachsel, B. Behrouz, M. Yue, J.E. Beevers, H.L. Melrose, M.J. Farrer, A comparative study of Lrrk2 function in primary neuronal cultures, Parkinsonism Relat. Disord. 16 (2010) 650–655.
- [15] F. Gillardon, Leucine-rich repeat kinase 2 phosphorylates brain tubulin-beta isoforms and modulates microtubule stability — a point of convergence in parkinsonian neurodegeneration? I. Neurochem. 110 (2009) 1514–1522.
- [16] M. Jaleel, R.J. Nichols, M. Deak, D.G. Campbell, F. Gillardon, A. Knebel, D.R. Alessi, LRRK2 phosphorylates moesin at threonine-558: characterization of how Parkinson's disease mutants affect kinase activity, Biochem. J. 405 (2007) 307–317.
- [17] P.N. Gandhi, X. Wang, X. Zhu, S.G. Chen, A.L. Wilson-Delfosse, The Roc domain of leucine-rich repeat kinase 2 is sufficient for interaction with microtubules, J. Neurosci. Res. 86 (8) (2008 Jun) 1711–1720, http://dx.doi.org/10.1002/jnr.21622.
- [18] F. Gillardon, Interaction of elongation factor 1-alpha with leucine-rich repeat kinase 2 impairs kinase activity and microtubule bundling in vitro, Neuroscience 163 (2009) 533-539
- [19] K. Habig, M. Walter, S. Poths, O. Riess, M. Bonin, RNA interference of LRRK2-microarray expression analysis of a Parkinson's disease key player, Neurogenetics 9 (2008) 83–94
- [20] R.M. Sancho, B.M. Law, K. Harvey, Mutations in the LRRK2 Roc-COR tandem domain link Parkinson's disease to Wnt signalling pathways, Hum. Mol. Genet. 18 (2009) 3955–3968
- [21] E. Mutez, L. Larvor, F. Lepretre, V. Mouroux, D. Hamalek, J.P. Kerckaert, J. Perez-Tur, N. Waucquier, C. Vanbesien-Mailliot, A. Duflot, D. Devos, L. Defebvre, A. Kreisler, B. Frigard, A. Destee, M.C. Chartier-Harlin, Transcriptional profile of Parkinson blood mononuclear cells with LRRK2 mutation, Neurobiol. Aging 32 (2011) 1839–1848.
- [22] D. Chan, A. Citro, J.M. Cordy, G.C. Shen, B. Wolozin, RAC1 rescues neurite retraction caused by G2019S leucine-rich repeat kinase 2 (LRRk2), J. Biol. Chem. 286 (18) (2011 May 6) 16140–16149, http://dx.doi.org/10.1074/jbc.M111.234005. Epub 2011 Mar 16.
- [23] A. Meixner, K. Boldt, M. Van Troys, M. Askenazi, C.J. Gloeckner, M. Bauer, J.A. Marto, C. Ampe, N. Kinkl, M. Ueffing, A quick screen for Lrrk2 interaction partners leucine-rich repeat kinase 2 is involved in actin cytoskeleton dynamics, Mol. Cell Proteomics 10 (1) (2011 Jan) M110.001172, http://dx.doi.org/10.1074/mcp.M110.001172. Epub 2010 Sep 27.
- [24] L. Parisiadou, C. Xie, H.J. Cho, X. Lin, X.L. Gu, C.X. Long, E. Lobbestael, V. Baekelandt, J.M. Taymans, L. Sun, H. Cai, Phosphorylation of ezrin/radixin/moesin proteins by LRRK2 promotes the rearrangement of actin cytoskeleton in neuronal morphogenesis, J. Neurosci. 29 (2009) 13971–13980.
- [25] E. Manser, T.H. Loo, C.G. Koh, Z.S. Zhao, X.Q. Chen, L. Tan, I. Tan, T. Leung, L. Lim, PAK kinases are directly coupled to the PIX family of nucleotide exchange factors, Mol. Cell 1 (1998) 183–192.
- [26] S. Bagrodia, S.J. Taylor, K.A. Jordon, L. Van Aelst, R.A. Cerione, A novel regulator of p21-activated kinases, J. Biol. Chem. 273 (1998) 23633–23636.
- [27] E.Y. Shin, C.S. Lee, T.G. Cho, Y.G. Kim, S. Song, Y.S. Juhnn, S.C. Park, E. Manser, E.G. Kim, BetaPak-interacting exchange factor-mediated Rac1 activation requires smgGDS guanine nucleotide exchange factor in basic fibroblast growth factor-induced neurite outgrowth, J. Biol. Chem. 281 (2006) 35954–35964.
- [28] E.Y. Shin, K.N. Woo, C.S. Lee, S.H. Koo, Y.G. Kim, W.J. Kim, C.D. Bae, S.I. Chang, E.G. Kim, Basic fibroblast growth factor stimulates activation of Rac1 through a p85 betaPIX phosphorylation-dependent pathway, J. Biol. Chem. 279 (2004) 1994–2004.
- [29] M. Paus, Z. Kohl, N.M. Ben Abdallah, D. Galter, F. Gillardon, J. Winkler, Enhanced dendritogenesis and axogenesis in hippocampal neuroblasts of LRRK2 knockout mice, Brain Res. 1497 (2013 Feb 25) 85–100, http://dx.doi.org/10.1016/j.brainres. 2012.12.024. Epub 2012 Dec 25.
- [30] C. Hitz, P. Steuber-Buchberger, S. Delic, W. Wurst, R. Kuhn, Generation of shRNA transgenic mice, Methods Mol. Biol. 530 (2009) 101–129.
- [31] S. Delic, S. Streif, J.M. Deussing, P. Weber, M. Ueffing, S.M. Holter, W. Wurst, R. Kuhn, Genetic mouse models for behavioral analysis through transgenic RNAi technology, Genes Brain Behav. 7 (2008) 821–830.

- [32] J.P. Kapfhammer, H. Xu, J.A. Raper, The detection and quantification of growth cone collapsing activities, Nat. Protoc. 2 (2007) 2005–2011.
- [33] U. Bichelmeier, T. Schmidt, J. Hubener, J. Boy, L. Ruttiger, K. Habig, S. Poths, M. Bonin, M. Knipper, W.J. Schmidt, J. Wilbertz, H. Wolburg, F. Laccone, O. Riess, Nuclear localization of ataxin-3 is required for the manifestation of symptoms in SCA3: in vivo evidence. I. Neurosci. 27 (2007) 7418–7428.
- [34] T.D. Pollard, G.G. Borisy, Cellular motility driven by assembly and disassembly of actin filaments, Cell 112 (2003) 453–465.
- [35] H.Y. Heo, K.S. Kim, W. Seol, Coordinate regulation of neurite outgrowth by LRRK2 and its interactor, Rab5, Exp. Neurobiol. 19 (2010) 97–105.
- [36] C.L. Wang, L.M. Coluccio, New insights into the regulation of the actin cytoskeleton by tropomyosin, Int. Rev. Cell Mol. Biol. 281 (2010) 91–128.
- [37] A.J. Ridley, Rho GTPases and actin dynamics in membrane protrusions and vesicle trafficking, Trends Cell Biol. 16 (2006) 522–529.
- [38] O. Bernard, Lim kinases, Regulators of actin dynamics, Int. J. Biochem. Cell Biol. 39 (2007) 1071–1076.
- [39] P. Gunning, E. Hardeman, P. Jeffrey, R. Weinberger, Creating intracellular structural domains: spatial segregation of actin and tropomyosin isoforms in neurons, Bioessays 20 (1998) 892–900.
- [40] G. Schevzov, N.S. Bryce, R. Almonte-Baldonado, J. Joya, J.J. Lin, E. Hardeman, R. Weinberger, P. Gunning, Specific features of neuronal size and shape are regulated by tropomyosin isoforms, Mol. Biol. Cell 16 (2005) 3425–3437.
- [41] T. Fath, Y.K. Agnes Chan, B. Vrhovski, H. Clarke, N. Curthoys, J. Hook, F. Lemckert, G. Schevzov, P. Tam, C.M. Watson, P.L. Khoo, P. Gunning, New aspects of tropomyosin-regulated neuritogenesis revealed by the deletion of Tm5NM1 and 2, Eur. J. Cell Biol. 89 (2010) 489–498.
- [42] B. Bugyi, D. Didry, M.F. Carlier, How tropomyosin regulates lamellipodial actin-based motility: a combined biochemical and reconstituted motility approach, EMBO J. 29 (2010) 14–26.
- [43] L. Blanchoin, T.D. Pollard, S.E. Hitchcock-DeGregori, Inhibition of the Arp2/3 complex-nucleated actin polymerization and branch formation by tropomyosin, Curr. Biol. 11 (2001) 1300–1304.
- [44] S.J. Cherra III, E. Steer, A.M. Gusdon, K. Kiselyov, C.T. Chu, Mutant LRRK2 elicits calcium imbalance and depletion of dendritic mitochondria in neurons, Am. J. Pathol. 182 (2013) 474–484.
- [45] Y. Tong, A. Pisani, G. Martella, M. Karouani, H. Yamaguchi, E.N. Pothos, J. Shen, R1441C mutation in LRRK2 impairs dopaminergic neurotransmission in mice, Proc. Natl. Acad. Sci. U. S. A. 106 (2009) 14622–14627.
- [46] L. Had, C. Faivre-Sarrailh, C. Legrand, J. Mery, J. Brugidou, A. Rabie, Tropomyosin isoforms in rat neurons: the different developmental profiles and distributions of TM-4 and TMBr-3 are consistent with different functions, J. Cell Sci. 107 (Pt 10) (1994) 2961–2973.
- [47] E.Y. Shin, K.S. Shin, C.S. Lee, K.N. Woo, S.H. Quan, N.K. Soung, Y.G. Kim, C.I. Cha, S.R. Kim, D. Park, G.M. Bokoch, E.G. Kim, Phosphorylation of p85 beta PIX, a Rac/Cdc42-specific guanine nucleotide exchange factor, via the Ras/ERK/PAK2 pathway is required for basic fibroblast growth factor-induced neurite outgrowth, J. Biol. Chem. 277 (2002) 44417–44430.
- 48] A.K. Liou, R.K. Leak, L. Li, M.J. Zigmond, Wild-type LRRK2 but not its mutant attenuates stress-induced cell death via ERK pathway, Neurobiol. Dis. 32 (2008) 116–124.
- [49] I. Carballo-Carbajal, S. Weber-Endress, G. Rovelli, D. Chan, B. Wolozin, C.L. Klein, N. Patenge, T. Gasser, P.J. Kahle, Leucine-rich repeat kinase 2 induces alpha-synuclein expression via the extracellular signal-regulated kinase pathway, Cell. Signal. 22 (2010) 821–827.
- [50] K. Kalil, G. Szebenyi, E.W. Dent, Common mechanisms underlying growth cone guidance and axon branching, J. Neurobiol. 44 (2000) 145–158.
- [51] G. Szebenyi, E.W. Dent, J.L. Callaway, C. Seys, H. Lueth, K. Kalil, Fibroblast growth factor-2 promotes axon branching of cortical neurons by influencing morphology and behavior of the primary growth cone, J. Neurosci. 21 (2001) 3932–3941.
- [52] E.W. Dent, F. Tang, K. Kalil, Axon guidance by growth cones and branches: common cytoskeletal and signaling mechanisms, Neuroscientist 9 (2003) 343–353.